

January 01, 2008

## Methods of I/Q imbalance correction for packet-switched IEEE802.11-compliant OFDM radios

Jeffrey Ross Feigin  
*Northeastern University*

---

### Recommended Citation

Feigin, Jeffrey Ross, "Methods of I/Q imbalance correction for packet-switched IEEE802.11-compliant OFDM radios" (2008). *Electrical Engineering Dissertations*. Paper 12. <http://hdl.handle.net/2047/d10017562>

This work is available open access, hosted by Northeastern University.

# Methods of I/Q Imbalance Correction for Packet-switched IEEE802.11-compliant OFDM Radios

A Dissertation Presented

by

Jeffrey Ross Feigin

to

The Department of Electrical and Computer Engineering

in partial fulfillment of the requirements

for the degree of

**Doctor of Philosophy**

in

Electrical Engineering

in the field of

Communications and Signal Processing

**Northeastern University**

**Boston, Massachusetts**

October, 2008

## **Acknowledgments**

I would like to thank Professor Brady, as has been a truly exceptional educator, advisor, and friend, and I could not have completed this work without him. I am extremely grateful to my former supervisors and colleagues, specifically Dogan Gunes, Amit Burstein, Daniel Jamison, Peter Bacon, David Whitefield, Mark Comerford and Stan Swearingen, for their support and assistance so that I could provide for my family while pursuing this PhD work. I thank Professors Stojanovic and Salehi for serving on my committee and their valuable insights.

This work is dedicated to the memory of my grandfather Jack and the honor of my grandfather Bob; both clearly would have earned PhD's in their individual fields of Chemistry and Psychology, had circumstances been more fortunate. I am also extremely grateful to my wife, Kristina, for her encouragement and enthusiasm regarding this endeavor.

## Abstract

Most modern integrated circuit transceivers, especially wireless LAN, utilize a direct conversion radio architecture. While this approach is highly advantageous from the perspectives of cost and flexibility, there exist several performance impairments, including gain and phase imbalances between the in-phase (I) and quadrature (Q) of a transmitter (TX) or receiver (RX). The dissertation presents several signal processing methodologies for compensation of I/Q imbalance for a direct conversion packet-switched OFDM communications system, which accounts for TX I/Q imbalance, RX I/Q imbalance, phase/frequency error, and dispersive multipath fading. Both frequency dependent I/Q imbalance and frequency independent cases are considered, covering both multicarrier and narrowband modulation. The proposed estimation algorithms operate within the fully compliant framework of existing multi-user OFDM radio standards (802.11a). It is shown that these algorithms accurately estimate and correct transceiver I/Q imbalance on a packet-by-packet basis, all within the RX's digital baseband.

## Contents

Acknowledgments	2
Abstract	3
List of Figures	6
Chapter 1. Introduction	10
1. Current State of the Art In I/Q Imbalance Correction	12
2. Radio Architecture Comparison: Superheterodyne vs. Direct Conversion	14
3. Direct Conversion Impairments	18
4. Orthogonal Frequency Domain Multiplexing (OFDM)	20
5. Performance Impact of I/Q Imbalance	27
6. 802.11 WLAN Background	30
Chapter 2. Joint Channel, I/Q Imbalance, and CFO Estimation Using Linear Least Squares	34
1. System Model	34
2. Parameter Estimation	39
3. Compensation Algorithm	45
4. Numerical Results	45
5. Conclusions	47
Chapter 3. A Non-Linear Constrained Least Squares Approach	51
1. Introduction	51
2. System model	54

	CONTENTS	5
3.	Parameter Estimation	55
4.	Simulation Results	60
5.	Conclusions	61
Chapter 4.	A Solution for Frequency Dependent I/Q Imbalance	65
1.	Introduction	65
2.	System Model	67
3.	Estimation Approach	70
4.	Compensation Algorithm	72
5.	Simulation Results	73
6.	Conclusions	77
	Bibliography	79

## List of Figures

- 1 A Typical Superheterodyne Radio RX Architecture is depicted. This 'dual conversion' variant uses two local oscillators and one intermediate frequency stage, where channel filtering is performed. Here, the final baseband stage produces a complex output. 15
- 2 A direct conversion RX architecture utilizes quadrature separation at the first frequency translation stage. Typical transceivers operate over a broad range of frequencies, in which quadrature phase requirements must be met. Further, all channel selectivity is derived from the baseband lowpass filters and the baseband variable gain amplifiers operate over an extremely large range of gain settings; this is a large source of amplitude imbalance. 16
- 3 The Direct Conversion TX Architecture also operates over a broad range of frequencies, which is difficult to maintain adequate 90-degree quadrature phasing. Since the real and imaginary baseband paths are separate realizations, this architecture also exhibits amplitude imbalance. 17
- 4 An OFDM symbol is comprised of individual orthogonal carriers, where the peak frequency of each carrier is aligned with the nulls from all neighboring carriers. Each subcarrier is independently modulated, but contains the same symbol timing phase and period as all neighboring carriers. 21
- 5 The autocorrelation of the LTS for IEEE802.11a has an extremely sharp response at zero offset; This behavior allows accurate timing, phase/frequency, and multipath estimation. 24

- 6 RX I/Q imbalance produces an interference components that is represented by a degradation in SINR. Here, the SINR (in the absence of noise) is plotted versus amplitude imbalance, at various levels of I/Q Imbalance phase error. The identical result would occur for TXs error, while the combination of both TX and RX error would result in further degradation of SINR. 26
- 7 The top-level structure of an IEEE802.11a OFDM packet. 31
- 8 The preamble structure for an IEEE802.11a packet contains ten repetitions of the STS, two repetitions of the LTS, a header, then data symbols. 33
- 1 The cross correlation of the LTS with its complex conjugate is zero at  $t=0$ , and remains relatively small at all offsets while the autocorrelation of the LTS a sharp thumbtack function. These properties make this training sequence especially suitable for estimating multipath delay taps, even in the presence of I/Q imbalance. 35
- 2 The resultant signal to interference ratio (in the absence of noise) for the proposed algorithm is plotted as the RX amplitude imbalance is varied. Here, the frequency offset is 150 kHz, ten packets are simulated per amplitude imbalance value, and three scenarios are demonstrated: 1) basic estimation without multipath, 2) basic estimation with 150 ns of delay spread, and 3) ideal CFO estimation. It is demonstrated that I/Q imbalance has little effect of phase/frequency offset (CFO) estimation for the 802.11a scenario. 41
- 3 The system model for the implementation of the packet switched TX/RX I/Q Imbalance estimation and correction algorithm. The RX correction is placed in-line with the digital baseband signal path such that the subsequent estimation and demodulation algorithms see diminished error after the first full-rank packet is received. 42
- 4 As the phase/frequency error between the TX and the RX approach zeros, the Grammian  $\mathbf{A}^T\mathbf{A}$  becomes badly conditioned and this problem is no longer full rank.

- The condition number for the Grammian (using the LTS) non-multipath and the L=4 (200 nS delay spread) case is plotted versus the frequency offset. Note: 240 KHz is equivalent to +40 ppm at 5.8 GHz. 43
- 5 The signal to interference ratio (in the absence of noise) for the proposed algorithm is plotted versus frequency offset in the presence of I/Q imbalance (TX Error of .5dB/ $-5^\circ$ , RX Error of .9dB/ $5^\circ$ , and Delay Spread of 200ns) 44
- 6 Comparison of algorithm performance with a 15 ppm Frequency Offset (90 KHz) and modest I/Q imbalance (TX Error of .1dB/ $-1^\circ$ , RX Error of .9dB/ $4^\circ$ , and Delay Spread of 150ns). 48
- 7 Algorithm performance with a 15 ppm Frequency Offset (90 KHz) and severe I/Q imbalance (TX Error of .5dB/ $-5^\circ$ , RX Error of .9dB/ $4^\circ$ , and Delay Spread of 150nS). 49
- 8 Comparison of algorithm performance with a 0 ppm (Synchronous) Frequency Offset, TX Error of .5dB/ $-5^\circ$ , RX Error of .9dB/ $4^\circ$ , and Delay Spread of 150ns, using a historical RX Estimate 50
- 1 Output SINR vs. SNR for various correction schemes using 802.11a OFDM Modulation in the presence of 150nS of multipath delay spread, .8dB/ $5^\circ$  TX I/Q imbalance, and  $-.9dB/5^\circ$  RX I/Q imbalance, and a 15 ppm frequency rotation. 62
- 2 Comparison of Output SINR vs. SNR for the proposed correction scheme versus various other works, when applied to this particular system model. This simulation includes 150nS of multipath delay spread, .5dB/ $5^\circ$  TX I/Q imbalance, and  $-.9dB/5^\circ$  of RX I/Q imbalance, and a 15 ppm frequency offset. 63
- 3 This simulation, unlike those represented in the previous figures, considers the multiuser scenario where each received packet emanates from a different TX. The RX I/Q imbalance parameters are  $-.9dB/5^\circ$  while each packet has a TX I/Q imbalance

that is uniformly distributed between the interval  $[-1, 1]dB$  and  $[-5, 5]$ degrees. It is shown, according to the resultant output SINR versus input SNR, that the multiuser packer-switched scenario requires critical algorithmic consideration for proper operation.

64

- 1 Various Orthogonal Frequency Domain Results for the  $\gamma$  Delay Tap Parameters where Only One Tap is Populated with a One. This Demonstrates that the Time Domain Delay-Tap Model is an Effective Means to Exploit Frequency Coherence and is Well-Suited for Ripple Functions. 69
- 2 The Convergence Behavior of the Gradient Descent Algorithm at Various SNRs. 72
- 3 The Results of of Frequency Dependent Imbalance Estimation versus the Actual Imbalance are shown at Various SNRs. It is Also Shown that the Averaged Result of Five Unique Estimates at an SNR of 15 dB Provides an Excellent Estimate. 75
- 4 Simulation Results for Various I/Q Imbalance Correction Algorithms in the Packet Switched Scenario where the RX Contains Severe ( $\pm 0.5$  dB) of Frequency Dependent Amplitude Imbalance Across the Channel Bandwidth. 76
- 5 Simulation Results for Various I/Q Imbalance Correction Algorithms in the Packet Switched Scenario where the RX Contains Mild ( $\pm 0.1$  dB) of Frequency Dependent Amplitude Imbalance Across the Channel Bandwidth. 77
- 6 A Comparison of the Proposed Algorithm and Tander07 in the Packet Switched Scenario where the RX Contains Severe ( $\pm 0.5$  dB) of Frequency Dependent Amplitude Imbalance Across the Channel Bandwidth. 78

## CHAPTER 1

### **Introduction**

With the rapidly growing consumer demand for broadband wireless data communications and broadcasting (including WIMAX, WLAN, UWB, DVB, DAB, DRM, etc.), wireless system designers and network operators must efficiently transfer tremendous amounts of data with limited electromagnetic spectra and power. Users of such systems require a very high level of performance and flexibility, while device portability, battery life and cost are key constraints for client devices. Furthermore, such systems operate under non-line-of-sight (NLOS) channel conditions where the received signal suffers from strong multipath interference.

OFDM modulation enables lower cost and current consumption while supporting high spectral efficiency through dispersive channels, and it is the predominant modulation format for many wireless communications systems. Additionally, a direct conversion radio architecture provides the potential for excellent current consumption, size, and radio performance, and it inherently allows a great degree of channel bandwidth flexibility. However, uncalibrated direct conversion transceivers suffer from I/Q imbalance. For example, unmitigated I/Q imbalance causes channel estimation error, which introduces further distortion to the equalizer output.

Many OFDM systems, particularly those deployed by professional network service providers, utilize radio architectures that exhibit little or no I/Q imbalance. However, most consumer electronic radio systems such as WLAN and some forms of WIMAX utilize direct conversion radios for both the TX and RX, and do have significant I/Q imbalance. Since the network timing and radio channel estimation sequences are extremely short (on the order of

microseconds) for packet-radio networks, such radio systems rely upon digital-domain signal processing to derotate the random phase/frequency error that exist between nodes. For consumer electronic radio, it is not usually practical to implement a direct conversion RX in packet-switched systems that has a synchronous carrier reference. Therefore, a generalized packet-based direct conversion communication system model must account for the combination of: 1) TX I/Q imbalance, 2) dispersive multipath, 3) phase/frequency offset, and 4) RX I/Q imbalance, in which all but the RX parameters change on a packet-by-packet basis.

This work, unlike other works, considers the packet-switched scenario where multiple nodes communicate with one another. Our work is a significant contribution to the state of the art in that this algorithm is capable of estimating both TX and RX I/Q imbalance parameters on a packet-by-packet basis in the presence of (or lack of) a phase/frequency error. This scenario exists in all 802.11 networks, where each received packet, whether from an intended or unintended source (because the channel is shared), has a possibly different TX I/Q imbalance and carrier frequency offset (CFO) parameters, which must be estimated and corrected during the training sequence. The estimation techniques investigated in this research, as well as their inherent partitioning of TX from RX parameters, have three unique implications not available together from other works: 1) an improved signal to noise-plus-interference ratio (SINR) due to the correction of the transmitted signal under the packet-switched scenario, 2) the possibility to send ‘advisory’ packets to the transmitting station such that it can correct the TX I/Q imbalance, and 3) the RX I/Q imbalance correction can be placed ahead of all other digital-domain signal processing algorithms. This work is also novel in that the low-rank problem (i.e., when CFO is small) is resolved using previously estimated RX parameters to reduce the rank of the estimate. Finally, this particular usage of a preamble-only technique itself is novel, in that it allows the necessary joint TX and RX parametrization under these packet-switched circumstances.

## 1. Current State of the Art In I/Q Imbalance Correction

There exists a large body of literature on the subject of I/Q imbalance, with substantial works that focus on OFDM in the presence of dispersive multipath. Some of these publications (such as [Xin05, Tub03, Val01, Bar07, Val05, Val05a, Par07]) focus on communications systems where only the RX suffers from I/Q imbalance (commercial subscriber-quality basestation TXs typically exhibit no I/Q imbalance). [Hai08, Hai07] extend the work of [Xin05] by proposing a solution to the low-rank problem that develops when the CFO is very small. [Ryk08] analyzes the equalization problem for this scenario while [Zou08] considers the effects under the joint TX/RX scenario in the context of space-time coding. Other publications also consider both TX and RX I/Q imbalance, but model synchronous systems with no CFO ([Tar07, Sch06]) .

Work [Tan07] considers the asynchronous case where both the TX and RX suffer I/Q imbalance in the presence of multipath, but requires a time-invariant channel and TX error parameters. The IEEE802.11a standard includes two equalizer training symbols per packet and provides two opportunities to update the specified LMS algorithm per packet [IEE99]. As the channel parameters and TX error parameters are likely to be quite unique for each received packet, in a multiuser environment (as each packet may have been sent by a unique TX), a sufficient number of training sequences would not be received for convergence of the estimation algorithm.

Work [Tan07] considers frequency dependent I/Q imbalance. Frequency dependent amplitude imbalance is primarily attributed to differences between the I-channel and Q-channel analog filters. Single-chip direct conversion works such as [Chi06, Zha05] as well as great many others utilize self-calibrating analog filters (presumably using a technique that adjusts the filter according to the system clock reference) while no similarly effective circuit-based I/Q balance correction technique exists. Although residual frequency-dependent error still

exists, this phenomenon may be considered a second-order effect in WLAN, but not for UWB where the channel bandwidth is approximately 30 times larger.

The multiuser scenario is particularly important for unlicensed networks such as IEEE802.11a Wireless LAN because these devices receive packets from multiple TXs, some of which are co-channel users. The network adapter must decode every packet, since this is only way to determine the intended recipient. As each TX has unique I/Q imbalance parameters and relative phase/frequency offset, the estimation results must be partitioned such that the phase/frequency and TX parameters are reset at the end of each incoming packet. It is of further importance to note that receive I/Q imbalance is a function of RX gain (this is because a direct conversion RX uses separate variable-gain paths for the I and Q channels)—each received packet, even from the same TX, is likely to result in a different RX gain setting. The multiuser scenario requires each packet to be considered separately and it is only possible to maintain a memory-based correction for RX parameters; this feature is further utilized to estimate the occasional low rank packet.

The proposed algorithms operate within the framework of any OFDM standard without the need for any special provisions or modifications. Using only the known channel training sequence, these algorithms estimate both the TX and RX I/Q imbalance parameters in the presence of CFO and dispersive multipath. Most importantly, these techniques rely solely upon the preamble interval of the incoming packet, even when the packet emanates from a unique TX with CFO and I/Q imbalance parameters in which there is no historical knowledge. This algorithm is executed until a sufficient I/Q imbalance vs. gain correction function is built within the RX, but continues to run, at a reduced level of complexity, for TX quadrature estimation and correction. Upon successful reception of only a few packets the RX I/Q error converges and hence there exists minimal effect upon the CFO estimation algorithm.

## 2. Radio Architecture Comparison: Superheterodyne vs. Direct Conversion

The goal of a radio RX is to amplify and translate signals, in the presence of various categories of background noise and interference, to levels and forms where the information can be recovered to a specified metric of reliability. There exists two main categories of architectures deployed in commercial radio communications systems: Superheterodyne and Direct Conversion. The former indicates that there exists an intermediate frequency stage between the baseband analog waveform and the TX/received radio frequency (RF) signal, while the latter indicates a direct translation between RF and baseband. Approaches such as direct-IF sampling and low-IF sampling are derivatives or hybrids of the Superheterodyne and Direct Conversion approaches.

Analytically, the output of an ideal complex modulator (TX), regardless of the architecture may be represented as

$$(1) \quad z_{T_{ideal}}(t) = \text{Re} \{ z(t)e^{j\omega_T t + \phi_T} \},$$

where  $z(t)$  is the complex baseband modulation,  $\omega_T$  is the carrier frequency and  $\phi_T$  represents the phase of the carrier. Similarly the output of an ideal complex down converter (RX) is represented as

$$(2) \quad z_{R_{ideal}}(t) = LPF \{ z_C(t)e^{-j\omega_R t} \}$$

Here,  $z_C(t)$  is the signal present at the antenna of the RX,  $\omega_R$  is the down conversion frequency, and the  $LPF \{ \cdot \}$  function represents a lowpass filter operation that removes spectral components not centered about DC. Equations 1 and 2 are simplified mathematical descriptions that represent the input-output relationships of a TX and RX, respectively. The actual implementation often includes intermediate steps such as partial frequency conversions,

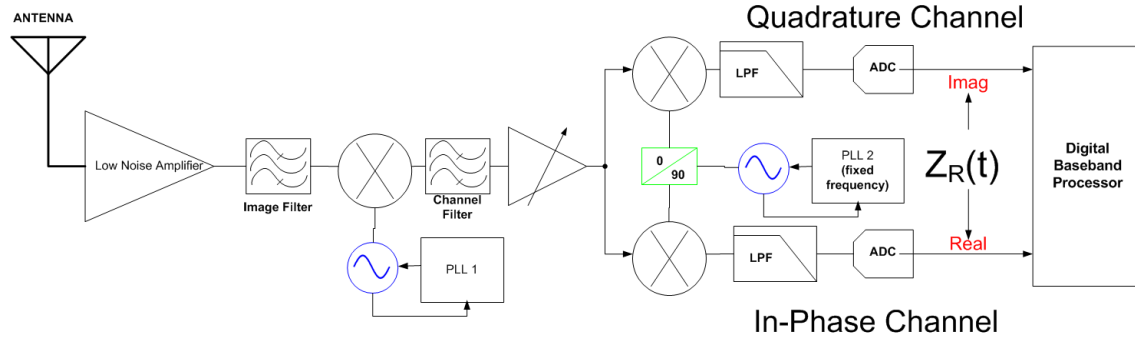


FIGURE 1. A Typical Superheterodyne Radio RX Architecture is depicted. This 'dual conversion' variant uses two local oscillators and one intermediate frequency stage, where channel filtering is performed. Here, the final baseband stage produces a complex output.

intermediate filters, and operations that independently act upon the real and imaginary components of the waveform.

**2.1. Superheterodyne Radio Architecture.** The superheterodyne technique was patented in 1918 by Edwin Armstrong as a means to overcome the difficulties associated with applying tremendous amplification to extremely weak radio signals. Though few of the limitations of 1918 electronic circuitry exists today (such as the ability to produce gain at high frequencies), this topology still offers highly desirable characteristics— Figure 1 depicts such a superheterodyne radio architecture. The foremost advantage is that the system gain is partitioned across multiple non-harmonically related frequencies; the fact that no one frequency stage exhibits more than a fraction of the total system gain greatly reduces the likelihood of instability. A second advantage is that because a possibly wide range of input frequencies is translated to just one specific passband at the intermediate frequency stage, a single off-chip filter (which achieves very high levels of performance not attainable through integrated circuit techniques) is implemented to act as a high dynamic range channel filter; subsequent amplification and signal processing is far easier once potentially strong interference signals are removed. The third advantage is that because the intermediate frequency

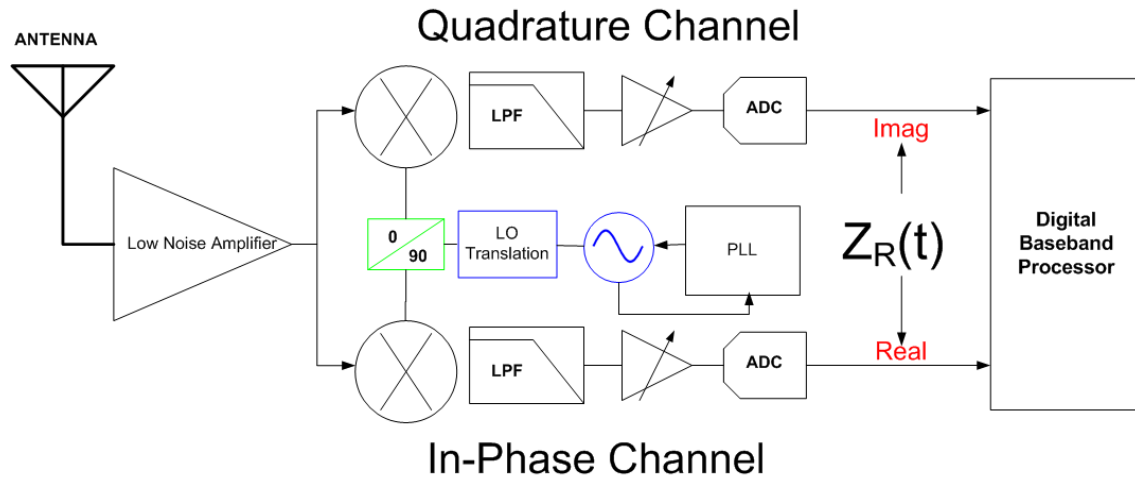


FIGURE 2. A direct conversion RX architecture utilizes quadrature separation at the first frequency translation stage. Typical transceivers operate over a broad range of frequencies, in which quadrature phase requirements must be met. Further, all channel selectivity is derived from the baseband lowpass filters and the baseband variable gain amplifiers operate over an extremely large range of gain settings; this is a large source of amplitude imbalance.

stage is bandpass coupled to the final stage, DC offsets caused by the first mixer do propagate through high-gain signal path; even small DC offsets could drive single-stage amplifiers with similar gains as a superheterodyne RX into blind saturation. Finally, the fact that almost all of the gain occurs in the real signal path (before quadrature separation) and that the quadrature separation operates a static low frequency, I/Q imbalance (amplitude and phase) is relative easy to manage. In summary, the superheterodyne radio architecture is an excellent technique for producing well-behaved and high-performance radio architectures.

**2.2. Direct Conversion Radio Architecture.** The Direct Conversion radio architecture (see Figure 2 and Figure 3) is simpler than superheterodyne– it lends itself well to monolithic integration. With careful planning and consideration, it is possible to build direct conversion transceivers that meet very demanding performance requirements. However, the issues inherently solved by the superheterodyne architecture must be handled in different ways. These single-chip transceivers are prevalent in markets such as Wireless LAN,

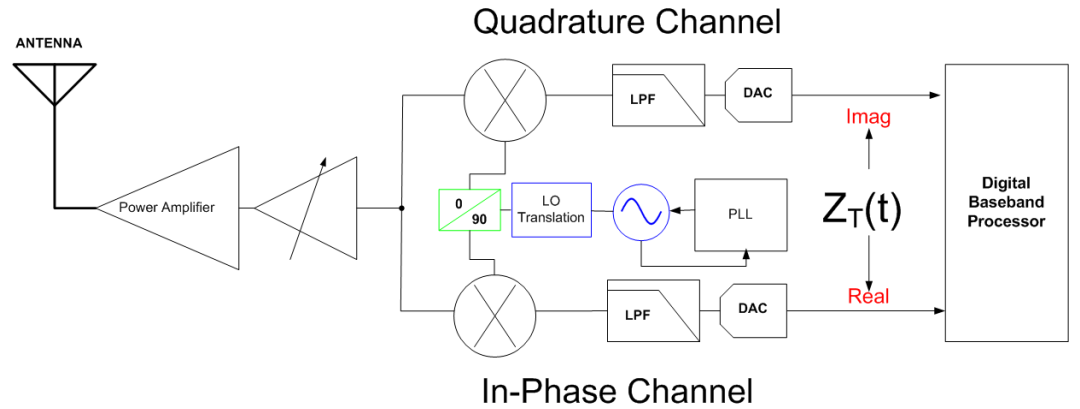


FIGURE 3. The Direct Conversion TX Architecture also operates over a broad range of frequencies, which is difficult to maintain adequate 90-degree quadrature phasing. Since the real and imaginary baseband paths are separate realizations, this architecture also exhibits amplitude imbalance.

WIMAX, and the various cellular standards (including 3G and 4G) due to their low cost and small form factors.

The architecture of a radio RX is based upon consideration that the desired signal (which ranges in magnitude from extremely small to extremely large) exists in the presence of adjacent and co-channel signals whose magnitudes could be significantly larger. The direct conversion transceiver must operate over a broad range of frequencies but no suitable channel filter technology (in existence today) is capable of being tuned in the same fashion. Therefore, the downconversion mixers (whose linearity is directly coupled to current consumption), are exposed to a wide dynamic range of received signals at various offsets from the desired carrier. Should the cumulative waveform, comprised of its various spectral components, drive these mixers beyond their linear operating range, the desired signal is irrecoverably lost. Low-power direct conversion RXs utilize only the minimum amount of RF gain required to overcome the noise and loss of the mixers; the remainder of the system gain is produced after this frequency conversion.

Once the RF signal is linearly translated to its quasi-synchronous complex baseband components, fixed low pass filters serve as the RF channel filter. This channel filter is

comprised of a complex pair of high-order low pass filters that act separately upon the real and imaginary paths. Now that off-channel spectral energy is removed, the desired signal is amplified by a factor of up to 70 dB or more by variable gain, but limited dynamic range, amplifiers. The gain of each these independent amplifiers is set so that the resultant output waveforms match the even more limited dynamic range of the analog to digital converters (ADCs).

### 3. Direct Conversion Impairments

**3.1. I/Q Imbalance Impairments.** There exist two major impairments to the accuracy of the transmitted/received waveform— amplitude imbalance and quadrature phase error. The amplitude imbalance results from the fact that real and imaginary paths exist as separate entities in the RX/TX, but is exacerbated in the RX by the degree and the control range of baseband variable gain amplifiers. Amplitude imbalance in a RX is a function of gain, while usually more static in a TX.

Quadrature phase error results in a up/down conversion error where the real and imaginary components of the transmitted baseband-equivalent or received baseband signal become somewhat correlated. Ideally, the (LO) sinusoids that is associated with the 'quadrature' mixer (the imaginary path) has a phase relationship of -90 degrees as compared to the 'in-phase' mixer. However, any deviation from the -90 degree phase relationship these two paths represents quadrature phase error. Quadrature up/downconversion, while also commonly utilized in superheterodyne radio architectures, is more problematic in Direct Conversion since this phase separation must be maintained over a broad range of RF channels rather than a single intermediate frequency that the much lower than that of the carrier.

The result of I/Q imbalance (amplitude and phase) is that, relative to the RXs (or TXs) own LO phase and frequency, the baseband (or baseband equivalent) waveform exists in the presence of a phase-rotated version of its own complex conjugate. It is observed that the

spectra of the baseband waveform exists in the presence of its own spectral mirror-image, when this type of distortion is present.

**3.2. Additional Direct Conversion LO and DC Offset Considerations.** The most significant difficulty in the implementation of single-chip direct conversion transceivers is the fact that such technology offers only a finite amount of component-to-component (i.e., transistors, inductors, resistors, capacitors, etc.) isolation and matching. This means that the three ports of a mixer (input, LO, and output) are directly coupled to some degree. Furthermore, the signals produced by the LO, comprised of a tunable Voltage Controlled Oscillator (VCO) is present on all ports of the mixer, as well. Finally, there exists coupling between the antenna and the VCO. The results of the coupling effects are catastrophic when ignored.

In a RX, the presence of the LO signal at multiple ports of the mixer (this is equivalent to mathematical squaring), limited port-to-port isolation, and device mismatch result in a continuous DC component at the mixer's output. VCO and LO leakage through the antenna results and DC offsets that are a function of low noise amplifier (LNA) gain and antenna loading; these DC offsets are dynamic, hence difficult to anticipate. Any such DC offset, whether dynamic or static can easily overload the subsequent variable gain amplifier (VGA) and ADC stages such that no useful information is present in the digital domain.

RX static DC offsets are commonly removed by introducing some form of high-pass response to the output of the mixers. One technique utilizes a function that moves the s-plane zeros in a specific time sequence in order to rapidly remove the DC error, then hold that DC value without interfering with the signaling spectra. Another technique utilizes DAC-based DC nulling signal at the input of the VGAs.

RX Dynamic DC offsets, however are very problematic since they are not predictable and can occur during time intervals where offset cancellation circuitry would interfere with the detectability of the signal. The best strategy regarding dynamic DC errors is to minimize

their occurrence; careful LO architectures, layout, and differential signaling help to reduce direct VCO coupling. The use of a VCO frequency that bears a non-integer relationship with the LO signal is a critical architectural choice that minimizes such dynamic coupling problems.

TX baseband DC offsets tend to be static, and result in LO feed through (carrier leakage). These errors are easily nulled by offsetting the I-Channel and Q-Channel DAC's such that minimum TX energy is detected at the power amplifier when no modulation information is presented.

The transceiver modulation phase stability is another key issue in direct conversion design. LO frequency translation (i.e., a 3/2 or 3/4 divide ratio) reduces phase disturbances since the very sensitive VCO is less coupled to the stages of the transceiver that exhibit load changes as they are adjusted. As a VCO is a quasi-linear circuit that contains positive feedback at a specific frequency, it is tremendously sensitive to any energy that bears an integer frequency relationship (especially energy that is a multiple of the VCO frequency). In the TX, such a frequency translation is even more crucial, as the modulated signal components will cause an unstable signal phase due this undesirable feedback.

#### 4. Orthogonal Frequency Domain Multiplexing (OFDM)

OFDM is a technique that divides the utilized spectra in many orthogonal carriers; each carrier is modulated independently. The orthogonality arises from the fact that the symbol period is inversely equal to the carrier spacing— the nulls of each carrier ( $\sin(x)/x$  spectra) are precisely aligned with the peaks of all neighboring carriers. Figure 4 depicts an example of this orthogonal relationship between subcarriers. All symbols are transmitted concurrently, each with a bandwidth that is a fraction of the total utilized bandwidth; ideally, each subchannel is much smaller than the coherence bandwidth of the multipath channel.

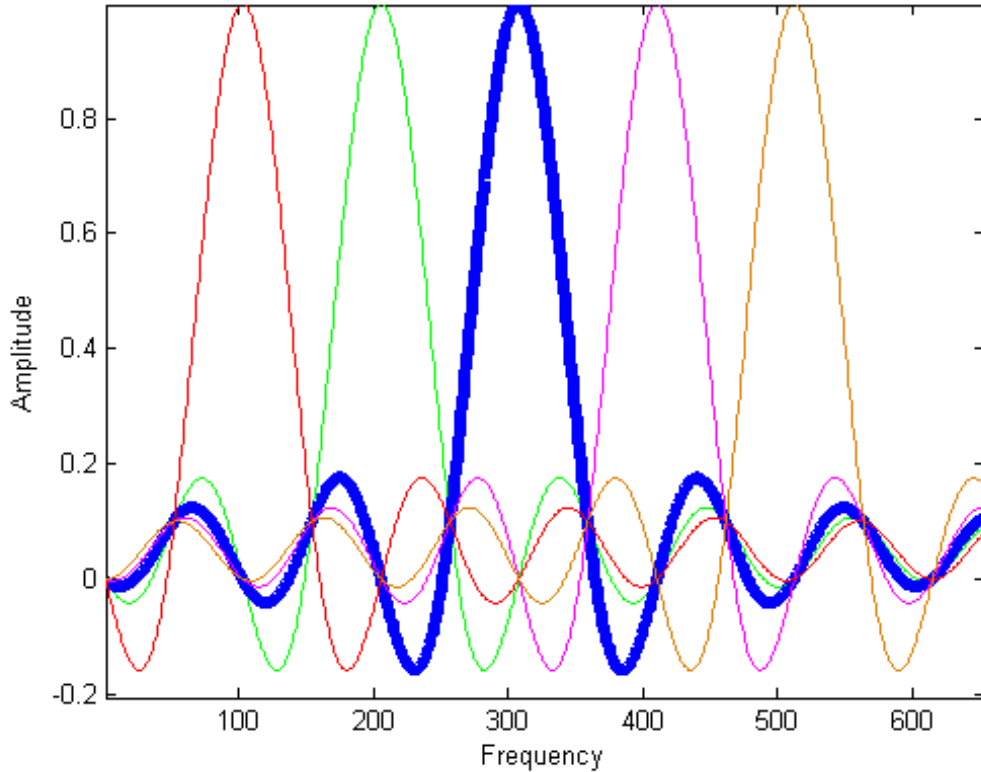


FIGURE 4. An OFDM symbol is comprised of individual orthogonal carriers, where the peak frequency of each carrier is aligned with the nulls from all neighboring carriers. Each subcarrier is independently modulated, but contains the same symbol timing phase and period as all neighboring carriers.

Each OFDM symbol, which contains the output of an inverse fast Fourier transform (IFFT) function that is preceded by a Guard Interval (whose purpose is to prevent inter-symbol interference). The most common technique is the Cyclic Prefix (CP), which means that the symbol is prepended with its own time domain extension. The symbol, itself, contains individually modulated carrier tones that represents data symbols and pilot tones (for synchronization). Some frequency-domain bins, particularly those centered about DC and near the edges of the positive and negative spectrum, are left empty.

Analytically, an OFDM symbol is expressed as [Hei02]

$$(3) \quad s(n) = \frac{A}{N} \sum_{i=0}^{N-1} m_i(n) e^{\frac{j2\pi in}{N}}, 0 \leq n < N$$

where  $A$  is a scaling factor,  $N$  is the length of the symbol in samples,  $n$  is the sample number,  $i$  is the subcarrier index, and  $m_i(n)$  is constellation position (i.e. 64 QAM, BPSK, etc.) of the  $i^{\text{th}}$  subcarrier at sample index  $n$ . The cyclic prefix, which is a copy of the last  $p$  samples of the samples concatenated to the beginning of this symbol, is expressed as

$$(4) \quad s(n - k) = s(N + n - k), n - k \leq p$$

where  $p$  is the length of the prefix and  $k$  is an index value.

**4.1. Equalization.** As long as the time period of the CP is longer than the channel delay spread, OFDM equalization may be performed in the RX by applying complex weights to each of the frequency domain subchannels. This modulation format is intended for scenarios where the channel is time-invariant (at least for the duration of the packet) and the symbol parameters are set to accommodate a certain maximum delay spread. Under the assumption of time invariance and non line of sight (NLOS) signaling, the magnitude of each tap of the complex channel impulse response is considered to have a probability density function of

$$(5) \quad f_z(z) = \frac{z}{\sigma^2} e^{-\frac{z^2}{2\sigma^2}}.$$

In the case where a strong line of sight path does exist, the Rician model is used instead

$$(6) \quad f_z(z) = \frac{z}{\sigma^2} I_0\left(\frac{z\eta}{\sigma^2}\right) e^{-\frac{z^2 + \eta^2}{2\sigma^2}}$$

where  $I_0$  is the modified Bessel function of zeroth kind of order zero and  $\eta$  is the mean magnitude due to the line of sight path. Both Equation 5 and Equation 6 are parametrized by  $\sigma$  and have a certain delay spread. The inverse of this delay spread determines the coherence bandwidth. It is also important that this delay spread does not extend beyond the length of the OFDM cyclic prefix— this would cause energy from one OFDM symbol to interfere with that of the next symbol.

The most direct and simple method for estimating the frequency domain OFDM equalization taps is to compare the received long training sequence (LTS) with the known LTS; this is simply an estimate of the channel  $H^{-1}(\omega)$ . The two LTS symbols, however, are received in the presence of noise; averaging these two symbols results in a signal-to-noise ratio (SNR) improvement of only 3 dB. Further improvement is possible by also averaging neighboring subcarriers, but at the expense of reduce delay spread tolerance.

Further, the LTS, is known at the baseband of the TX, not its antenna. This  $H^{-1}(\omega)$  estimation technique does not account for the I/Q imbalance induced by the TX. Also, RX I/Q imbalance will greatly affect the accuracy of the result. Therefore, full knowledge of the RX and TX I/Q imbalance is required when performing OFDM channel equalization.

**4.2. Synchronization (Frequency, Phase, Time, and Gain).** Since each transceiver has a unique internal clock reference, each with its own unique error, there exists a relative error in both carrier frequency and sample/symbol timing between any two devices. Further, the radio channel induces a random distribution of carrier phase and signal amplitude. Finally, the absolute time of each packet transmission is random and this timing parameter must be estimated so that each fast Fourier transform (FFT) operation is aligned with one OFDM symbol. OFDM radio standards provide training sequences that exhibit extremely sharp correlation responses for the purpose of synchronization of phase, frequency, timing, and amplitude— Figure 5 shows the autocorrelation of the IEEE 802.11a Long Training Sequence.

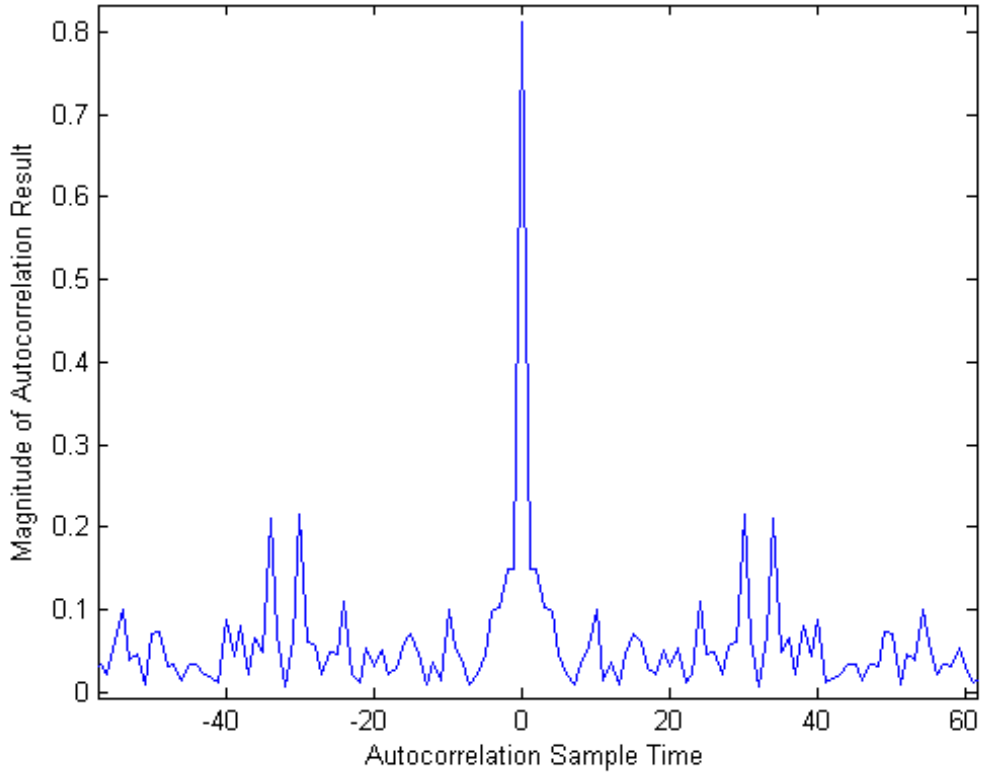


FIGURE 5. The autocorrelation of the LTS for IEEE802.11a has an extremely sharp response at zero offset; This behavior allows accurate timing, phase/frequency, and multipath estimation.

Timing alignment, denoted by  $t_s$  is determined by a sliding correlator window function such that

$$(7) \quad t_s = \underset{k}{\operatorname{argmax}} \left| \sum_{n=0}^{N-1} \tilde{z}(n+k_0) z^*(n) \right|^2.$$

Here  $n$  is the sample index,  $k_0$  is the sample offset that represents the start of the first training sequence,  $N$  is the length of the training sequence,  $\tilde{z}(n)$  is the received sequence,  $z(n)$  is the known transmitted training sequence.

Successful coherent detection requires that the received complex waveform is phase/frequency synchronous with that of the transmitted waveform. This is accomplished by use of both

training symbols and specific pilot tones within the OFDM symbol. WLAN OFDM systems use known, equally spaced, repeating training sequences; estimation of the unwrapped phase of each symbol, combined with knowledge of the time difference allows the RX to digitally compute and correct its relative phase and frequency error. The first step of phase/frequency estimation is mathematically described as

$$(8) \quad \tilde{R}_i = \sum_{n=0}^{N-1} \tilde{z}(n + k_i) z^*(n),$$

where  $k_i$  is a sample offset within received sequence that aligns the received training sequence in sample-time with  $z(n)$ , and  $i$  refers to the training sequence repetition number. The unwrapped phase result  $\arg(\tilde{R}_i)$  has the following relationship to phase/frequency difference between the TX and RX:

$$(9) \quad \arg(\tilde{R}_i) = (\omega_T - \omega_R)t_i + \phi_T + \epsilon(t_i).$$

As  $t_i$  is the time of each symbol and  $\epsilon(t_i)$  denotes the contribution of uncorrelated zero-mean wide-sense stationary noise that is contained within  $\tilde{z}(n)$ , the parameters for the phase/frequency error are found by estimating the slope and offset of Equation 9.

This technique has practical frequency estimation limits since large frequency errors will cause a modulus wrapping error in the phase of  $\tilde{R}_i$ . In the case of WLAN, both long and short training sequences are provided as well as strict limits for the maximum possible absolute frequency error, such that estimation requires a separate coarse and fine acquisition.

While the above technique produces an accurate estimate of the relative phase/frequency error between the TX and RX, there will still exist some small error. OFDM standards also include pilot tones (individual subcarriers that transmitted with a known pattern) that can be used to track the residual error on a symbol-by-symbol basis.

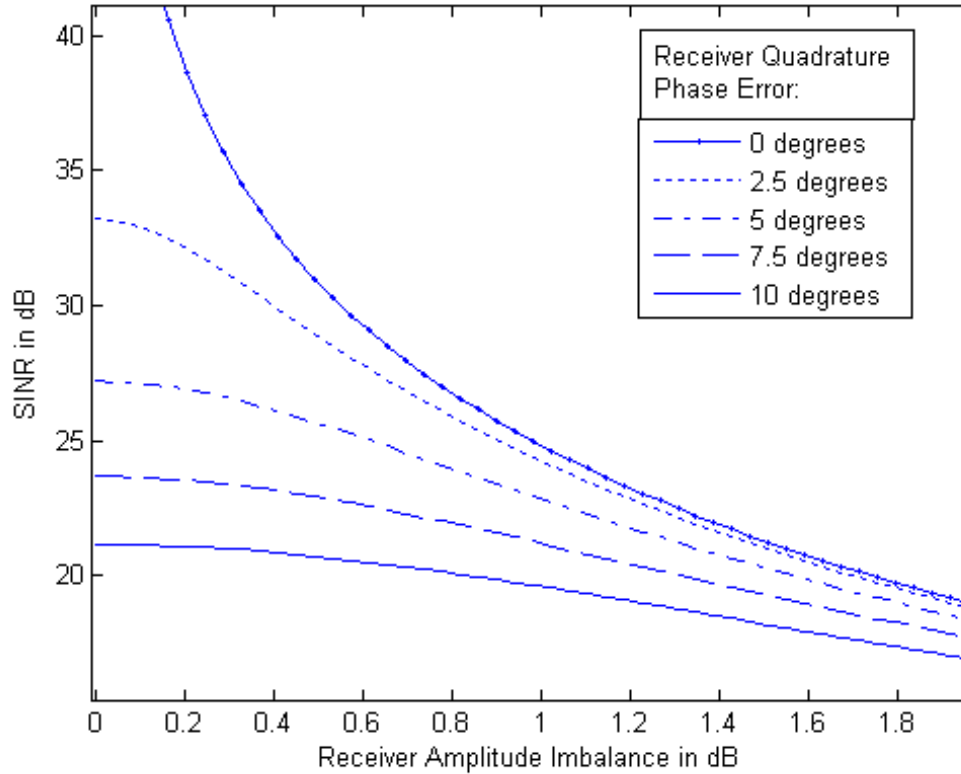


FIGURE 6. RX I/Q imbalance produces an interference components that is represented by a degradation in SINR. Here, the SINR (in the absence of noise) is plotted versus amplitude imbalance, at various levels of I/Q Imbalance phase error. The identical result would occur for TXs error, while the combination of both TX and RX error would result in further degradation of SINR.

Finally, since a typical ADC operates with a very limited dynamic range window, RX gain must be adjusted to accommodate the desired incoming waveform. This is accomplished by utilizing the information obtained from the correlation result,  $abs(\tilde{R}_i)$ , to make adjustments. Typically, the short training sequence is used, and such a scheme requires only 2-3 iterations before adequate convergence (the remaining 7-8 repetitions of the STS are used for coarse frequency acquisition and diversity antenna selection).

### 5. Performance Impact of I/Q Imbalance

I/Q imbalance is the combination of I/Q channel amplitude imbalance and LO phase error (the difference from 90-degrees between and I and Q LO signals). In a TX, the baseband-equivalent of the modulated carrier exists in the presence of its own phase-shifted complex conjugate. In the time domain, a RX that suffers from I/Q imbalance downconverts the complex conjugate of the modulated carrier as well as the desired waveform to baseband. In the frequency domain, this interference term (the complex conjugate of the desired waveform) is the phase-shifted, complex conjugate, and mirror-image of the intended spectra. The result of this conjugate error is a degradation in SINR; Figure 6 shows the exact relationship between I/Q Imbalance and SINR. Such non-linear distortion, unlike most other types of distortion and interference, is easily corrected, once properly characterized.

These analytical expression for I/Q imbalance in a direct conversion TX is derived from the basic expression for a complex modulator,

$$\begin{aligned}
 (10) \quad S_{T_{ideal}}(t) &= \text{Re} \{z(t)e^{j\omega_T t}\} \\
 &= \text{Re} \{z(t) [\cos(\omega_T t) + j \cdot \sin(\omega_T t)]\}.
 \end{aligned}$$

Since  $\text{Re} \{\xi\} = \frac{1}{2} [\xi + \xi^*]$ ,

$$(11) \quad S_{T_{ideal}}(t) = \text{Re} \{z(t)\} \cos(\omega_T t) - \text{Im} \{z(t)\} \sin(\omega_T t),$$

which directly describes the physical realization of the direct conversion TX. Considering an amplitude imbalance of  $a_T$ , whose value is the difference in gain between the I and Q channels, and a I/Q Imbalance phase error of  $\theta_T$ , which is the difference from 90 degrees between the real and imaginary LO signals, this expression becomes

$$(12) \quad S_T(t) = \operatorname{Re} \{z(t)\} \cdot \cos(\omega_T t) - \operatorname{Im} \{z(t)\} (1 + a_T) \cdot \sin(\omega_T t + \theta_T).$$

In exponential form, using the relationships

$$(13) \quad \begin{aligned} \cos(\xi) &= \frac{e^{j\xi} + e^{-j\xi}}{2} \\ \sin(\xi) &= \frac{e^{j\xi} - e^{-j\xi}}{2j} \end{aligned} ,$$

it is found that

$$(14) \quad S_T(t) = \operatorname{Re} \left\{ z(t) \left[ \frac{1 + (1 + a_T)e^{-j\theta_T}}{2} e^{j\omega_T t} + \frac{1 - (1 + a_T)e^{-j\theta_T}}{2} e^{-j\omega_T t} \right] \right\}$$

where it is interpreted that when  $a_T$  or  $\theta_T$  is non-zero, there will exist an interference product (the second term inside the brackets) in addition to the desired product (the first term inside the brackets). Again, considering that  $\operatorname{Re} \{\xi\} = \frac{1}{2} [\xi + \xi^*]$ , we find the baseband equivalent (assuming a synchronous carrier reference) of Equation 14 to be

$$(15) \quad z_T(t) = \frac{1}{2}(1 + (1 + a_T)e^{j\theta_T})z(t) + \frac{1}{2}(1 - (1 + a_T)e^{j\theta_T})z^*(t),$$

which means that the interference term is the the complex conjugate of the desired baseband modulation scaled by a complex factor,  $\frac{1}{2}(1 - (1 + a_T)e^{j\theta_T})$ .

Similarly, the expression for an imperfect RX (ignoring noise), including a phase and frequency offset from the TX, is derived from the ideal direct conversion RX,

$$(16) \quad \begin{aligned} z_{R_{ideal}}(t) &= \operatorname{LPF} \{z_C(t)e^{-j\omega_R t + \phi_R}\} \\ &= \operatorname{LPF} \{Z_C(t) [\cos(\omega_R t) - j \cdot \sin(\omega_R t)]\} \end{aligned} .$$

I/Q imbalance,  $a_R$  and  $\theta_R$ , amplitude and phase, respectively, are included such that

$$(17) \quad Z_R(t) = LPF \{Z_C(t) [\cos(\omega_R t) - j \cdot \sin(\omega_R t)]\}.$$

The exponential form of Equation 17 is expressed as

$$(18) \quad Z_R(t) = LPF \left\{ z_C(t) \left[ \frac{1 - (1 + a_R)e^{-j\theta_R}}{2} e^{j(\omega_R t)} + \frac{1 + (1 + a_R)e^{-j\theta_R}}{2} e^{-j(\omega_R t)} \right] \right\}.$$

Now, ignoring channel effects and noise, but considering that the TX frequency is not synchronous with the RX phase or frequency, the received baseband waveform is expressed as

$$(19) \quad Z_R(t) = \begin{aligned} & \frac{z(t)}{4} (1 + (1 + a_R)e^{-j\theta_R})(1 + (1 + a_T)e^{j\theta_T}) e^{j(\omega_T - \omega_R)t + j\phi_T} \\ & \frac{z^*(t)}{4} (1 + (1 + a_R)e^{-j\theta_R})(1 - (1 + a_T)e^{j\theta_T}) e^{j(\omega_T - \omega_R)t + j\phi_T} \\ & \frac{z^*(t)}{4} (1 - (1 + a_R)e^{j\theta_R})(1 + (1 + a_T)e^{-j\theta_T}) e^{-j(\omega_T - \omega_R)t - j\phi_T} \\ & \frac{z(t)}{4} (1 - (1 + a_R)e^{j\theta_R})(1 - (1 + a_T)e^{-j\theta_T}) e^{-j(\omega_T - \omega_R)t - j\phi_T} \end{aligned}.$$

Finally, as the asynchronous phase/frequency error is (ideally) removed, the received complex waveform is derotated such that resultant baseband signal is found:

$$(20) \quad \widetilde{z}(t) = \begin{aligned} & \frac{z(t)}{4} (1 + (1 + a_R)e^{-j\theta_R})(1 + (1 + a_T)e^{j\theta_T}) \\ & \frac{z^*(t)}{4} (1 + (1 + a_R)e^{-j\theta_R})(1 - (1 + a_T)e^{j\theta_T}) \\ & \frac{z^*(t)}{4} (1 - (1 + a_R)e^{j\theta_R})(1 + (1 + a_T)e^{-j\theta_T}) e^{-2j(\omega_T - \omega_R)t - 2j\phi_T} \\ & \frac{z(t)}{4} (1 - (1 + a_R)e^{j\theta_R})(1 - (1 + a_T)e^{-j\theta_T}) e^{-2j(\omega_T - \omega_R)t - 2j\phi_T} \end{aligned}.$$

Here, it is shown that the transmitted baseband waveform is received in the presence of three interference products. The first row of Equation 20 represents the desired waveform,

while the second and third rows are scaled versions the complex conjugate of  $z(t)$ , where the third term is rotating at a frequency and phase twice that of the difference between the TX and RX phase/frequency. The fourth term is a very weak, but asynchronous non-conjugate term.

SINR is defined as the ratio of signal level to noise and interference products. The resultant SINR, in dB for Equation 20 is:

$$(21) \quad SINR = 10\log_{10} \left[ \frac{|k_1|^2}{|k_2|^2 + |k_3|^2 + |k_4|^2} \right]$$

## 6. 802.11 WLAN Background

The IEEE 802.11 standard, originally ratified in 1997, is a set of specifications for Wireless Local Area Network (WLAN) communications that operates using primarily the 2.4GHz and 5 GHz unlicensed spectrum. Since its original inception, the standard has been regularly amended to include new improvements (many are not adopted by industry) in wireless modulation, power control, interference avoidance, coding, encryption, authentication, and medium access control technology. Each subsequent revision, where possible, mandates backwards device compatibility with predecessor technology.

WLAN technology is used by commercial network operators, corporate/commercial infrastructure, industrial, and residential users for a variety of purposes. Common applications include short-range (<100 meters) internet voice/data, local area networking, proprietary commercial communications (such as portable bar-code scanners and Point of Sale terminals), and machine-to-machine communications. These applications are implemented on computers, PDA's, handsets, industrial equipment, vending machines, and many other types of equipment. All such users, however, share common public spectra and must operate in the presence of other users and undesirable interference sources.

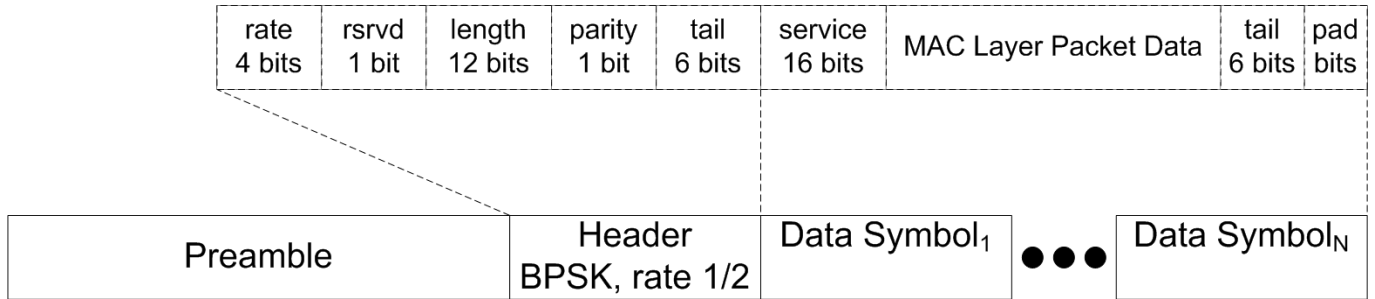


FIGURE 7. The top-level structure of an IEEE802.11a OFDM packet.

**6.1. PHY modes of operation.** The most basic physical layer (PHY) mode supported for current 2.4GHz (other modes did exist in the original specification, but are no longer relevant) 802.11 is Direct Sequence Spread Spectrum (DSSS). This modulation scheme is based upon BPSK or QPSK chips and provides a PHY data rate of 1 or 2 Mbps, respectively. The 802.11a amendment specifies 5 GHz OFDM operation (up to 54 Mbps) and does not require backwards compatibility to the 802.11 PHY. Amendment 802.11b is a subsequent modification of the original 802.11 specification for the 2.4 GHz band; its predominant mode includes additional higher-rate coding schemes that continue to utilize QPSK. 802.11b continues support of the original 1 and 2 Mbps mode, but also includes 5.5 and 11 Mbps PHY rates. The next relevant amendment is 802.11g, where the identical 802.11a OFDM modulation scheme is adopted for the 2.4 GHz band. This is the prevalent modulation format used in WLAN devices at this date— this work focuses on that particular OFDM format.

Future 802.11 amendments are currently under development, most notably the 802.11n standard. The 802.11n standard is intended to support PHY data rates of up to 600 Mbps, by utilizing greater bandwidths and Multiple Input Multiple Output (MIMO) communications techniques as enhancements to the underlying OFDM modulation. The 802.11n standard is currently expected to be finalized in March of 2009.

## 6.2. OFDM specific 802.11 background.

Data Rate (Mbps)	Modulation Constellation	Coding Rate	Bits per OFDM Symbol
6	BPSK	1/2	24
9	BPSK	3/4	36
12	QPSK	1/2	48
18	QPSK	3/4	72
24	16-QAM	1/2	96
36	16-QAM	3/4	144
48	64-QAM	2/3	192
54	64-QAM	3/4	216

TABLE 1. The various data rates, constellations, and coding rates supported by 802.11a/g OFDM operation

The 802.11a standard (which is incorporated in the 802.11g standard) specifies OFDM modes that support data rates of 6, 9, 12, 18, 24, 36, 48, and 54 Mbps. Table 1 lists each possible mode and the corresponding parameters. All data rates utilize a common OFDM symbol format that is based upon a 64-point IFFT. Forty-eight of the bins contain these data carriers while 4 are pseudorandom BPSK pilots while the remaining bins are left empty.

An 802.11a OFDM transmission, which is a train of individual time-domain symbols (see Figure 7), starts with synchronization sequences. 802.11a OFDM transmissions begin with ten repetitions of a Short Training Sequence (STS), then two repetitions of the Long Training Sequence (LTS); Figure 8 depicts this preamble structure. The STS is one quarter the length of a regular symbol while the LTS is the same length as the IFFT size. Following the LTS is the header symbol (which contains information about the subsequent modulation and coding rate) then a series of regular data symbols. Preceding the LTS symbols is a cyclic prefix that is half the length of the LTS, itself. The CP that precedes each data symbol is one quarter the length each such symbol.

**6.3. 802.11 MAC Considerations.** The fundamental MAC (Medium Access Control) utilized by the 802.11 standard is Carrier Sense Multiple Access with Collision Avoidance (CSMA/CA). This means that each station listens to the channel to determine if it is in

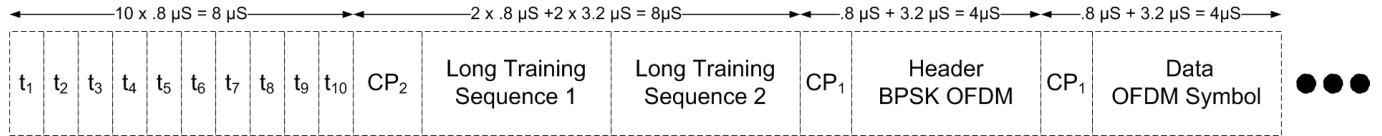


FIGURE 8. The preamble structure for an IEEE802.11a packet contains ten repetitions of the STS, two repetitions of the LTS, a header, then data symbols.

use before transmitting and randomizes the amount of delay before attempting to seize a newly relinquished channel. The random delay interval is set according to an algorithm that intends to less aggressively acquire the channel when traffic intensity is high. This scheme suffers from the limitation that not all stations are able to detect energy from all other stations (hidden nodes) and collisions are still common. An enhancement to this scheme is the Request-to-Send/Clear-to-Send (RTS/CTS) algorithm that coordinates each transmission with the recipient station such that all listening peer stations refrain from transmitting during a particular interval.

There exists two fundamental modes of operation at the network level: ad hoc and access point mode. The ad hoc mode is a multiuser scenario where stations connect directly to other stations and communicate as peers. Access point mode means that individuals nodes may only communicate with an access point (the access point usually acts as a gateway to a wired network), even when data is intended for a peer that is also operating on the same subnetwork. While the 802.11 standard specifies timing and network coordination protocols in great detail, such channel use procedures are not coordinated with stations operating on other networks.

The 802.11 channel is shared among many users and possibly many unrelated networks of users; one particular station is likely to receive packets in which it is not the intended recipient. In general, a WLAN node is required to decode at least the beginning of every packet it receives in order to determine whether to discard the packet or pass the information to higher layers of the network protocol stack.

## CHAPTER 2

# Joint Channel, I/Q Imbalance, and CFO Estimation Using Linear Least Squares

In this chapter, a system model is presented which includes the effects of TX I/Q imbalance, RX I/Q imbalance, phase/frequency error, as well as a dispersive multipath channel. A linear least squares estimation (LLSE) approach is then developed to estimate the channel and imbalance parameters. Finally, a correction scheme is presented and simulation results compare the performance to that of previous work

### 1. System Model

The complex envelope of the undistorted transmitted signal  $z(t)$  is related to the complex envelope of the TX output  $z_T(t)$ , then to the complex envelope of the noiseless signal at the input to the RX  $z_C(t)$ , and finally to the noiseless complex baseband received signal after down-converting  $z_R(t)$ . While these relationships hold for arbitrary  $z(t)$ , we are especially interested in  $z(t)$  being a known, training sequence (e.g. the Long Training Sequence (LTS) in the IEEE802.11a standard) so that the relevant parameters of I/Q imbalance, phase/frequency error, and dispersive multipath can be estimated at the RX.

The LTS has a thumbtack-shaped autocorrelation function and a low correlation with its complex conjugate for all delays (I/Q imbalance distortion components are primarily the complex conjugate of the desired signal components). This type of waveform facilitates the estimation of I/Q imbalance parameters, as will be shown in 2. Figure 1 shows plots of these correlation results at a range of time offsets.. Without loss of generality, we set the phase of the RX's in-phase branch to zero, and we define the complex envelope  $c(t)$  of a passband

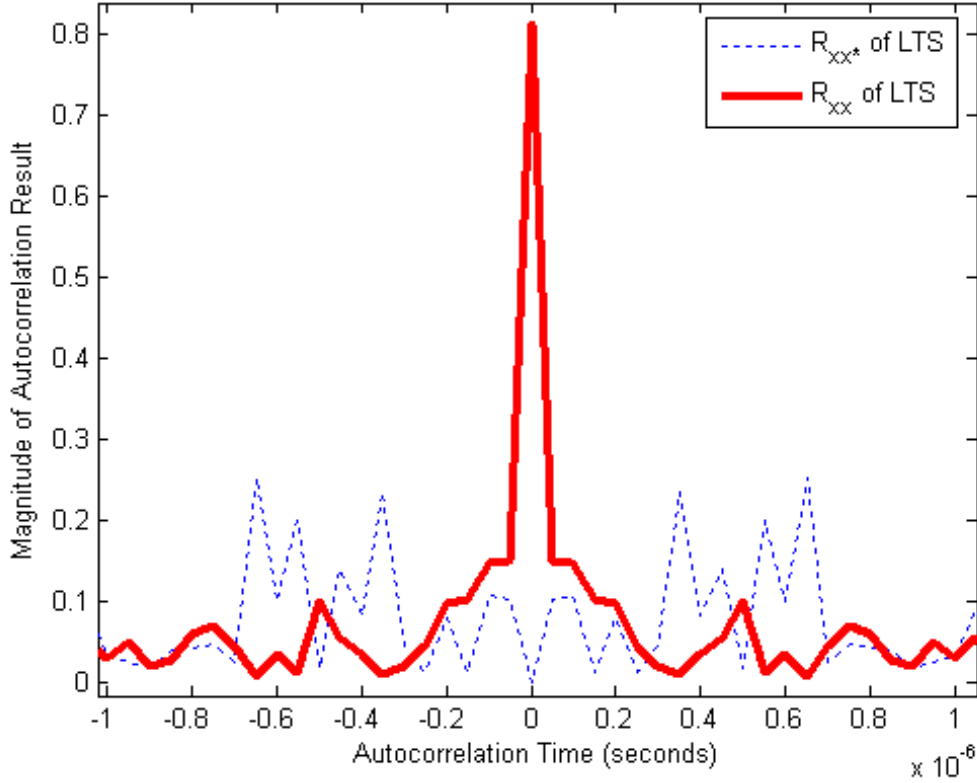


FIGURE 1. The cross correlation of the LTS with its complex conjugate is zero at  $t=0$ , and remains relatively small at all offsets while the autocorrelation of the LTS a sharp thumbtack function. These properties make this training sequence especially suitable for estimating multipath delay taps, even in the presence of I/Q imbalance.

signal  $x(t)$  with respect to the RX's in-phase branch,  $x(t) = \text{Re}(c(t)e^{j\omega_R t})$ . Here,  $\omega_R$  is the radian carrier frequency of the RX. The noiseless TX output  $s(t)$  may be related to  $z(t)$  as

$$\begin{aligned}
 s(t) &= \text{Re}\{z(t)\} \cos(\omega_T t + \phi_T) - \text{Im}\{z(t)\} (1 + a_T) \sin(\omega_T t + \theta_T + \phi_T), \\
 &= \text{Re}\{z_T(t)e^{j\omega_R t}\}, \text{ where} \\
 (22) \quad z_T(t) &= \frac{1}{2}r(t)(1 + (1 + a_T)e^{j\theta_T})z(t) \\
 &\quad + \frac{1}{2}r(t)(1 - (1 + a_T)e^{j\theta_T})z^*(t), \text{ and} \\
 r(t) &= e^{j(\omega_T - \omega_R)t + j\phi_T}.
 \end{aligned}$$

Here  $a_T$  (resp.  $\theta_T$ ) denotes the relative amplitude (resp. phase) imbalance of the TX's quadrature branch, and  $\omega_T$  is the radian carrier frequency of the TX. Also,  $\phi_T$  is the phase offset between the in-phase branches of the TX and RX, and the function  $r(t)$  accounts for the instantaneous phase offsets between these branches.

The complex envelope  $h(t)$  of the impulse response is assumed to be invariant for the packet duration and results in the complex envelope  $z_C(t)$  of the noiseless signal at the input to the RX by convolution  $z_C(t) = \frac{1}{2}h \star z_T(t)$ , [Cou07] or

$$(23) \quad \begin{aligned} z_C(t) &\approx \frac{1}{2}r(t)(1 + (1 + a_T)e^{j\theta_T})h \star z(t) \\ &\quad + \frac{1}{2}r(t)(1 - (1 + a_T)e^{j\theta_T})h \star z^*(t). \end{aligned}$$

This approximation is valid if the support of  $h(t)$ ,  $S_h$ , satisfies  $(\omega_T - \omega_R)S_h \ll 2\pi$ . With each oscillator having a frequency stability of  $\pm 20$  ppm, and with  $S_h = 80$  ns and a carrier frequency of  $5.8$  GHz, this inequality becomes  $|(\omega_T - \omega_R)S_h| < 0.06 \ll 2\pi$ . Since the inequality is satisfied in practice, we will ignore the approximation in the following. The RX I/Q imbalance further distorts the down-converted signal, yielding the complex envelope  $z_R(t)$

$$(24) \quad \begin{aligned} z_R(t) &= r(t)k_1h \star z(t) + r(t)k_2h \star z^*(t) + \\ &\quad r^*(t)k_3h^* \star z^*(t) + r^*(t)k_4h^* \star z(t), \end{aligned}$$

where, ignoring a positive constant common to all terms,

$$(25) \quad \begin{aligned} k_1 &= \frac{1}{4}(1 + (1 + a_R)e^{-j\theta_R})(1 + (1 + a_T)e^{j\theta_T}), \\ k_2 &= \frac{1}{4}(1 + (1 + a_R)e^{-j\theta_R})(1 - (1 + a_T)e^{j\theta_T}), \\ k_3 &= \frac{1}{4}(1 - (1 + a_R)e^{j\theta_R})(1 + (1 + a_T)e^{-j\theta_T}), \text{ and} \\ k_4 &= \frac{1}{4}(1 - (1 + a_R)e^{j\theta_R})(1 - (1 + a_T)e^{-j\theta_T}). \end{aligned}$$

Here,  $a_R$  (resp.  $\theta_R$ ) denotes the relative amplitude (resp. phase) imbalance of the RX's quadrature branch. We will neglect the last term in Equation 40 as  $k_4$  is strongly dominated

by the three other coefficients. For example, for typical values of amplitude and phase imbalances,  $|k_4|/\max(|k_2|, |k_3|) \approx \frac{1}{2}\min(|a_T|, |a_R|)$ . As a result of the effects of I/Q imbalance at both TX and RX, phase offset, frequency offset, and channel distortion, we have the following relationship between the received noisy baseband signal  $\tilde{z}(t)$  and its ideal counterpart  $z(t)$ ,

$$(26) \quad \tilde{z}(t) = r(t) (k_1 h \star z(t) + k_2 h \star z^*(t)) + r^*(t) k_3 h^* \star z^*(t) + n(t), \quad 0 \leq t \leq N - 1,$$

where  $n(t)$  denotes zero-mean, complex-circular wide-sense stationary white noise. In the special case when TX imbalance may be ignored,  $k_2 = 0$ . With the additional restriction of perfect oscillator synchronization, we have  $r(t) = 1$ , and  $\tilde{z}(t) = k_1 h \star z(t) + k_3 h^* \star z^*(t) + n(t)$ . Finally, in the absence of channel distortion, oscillator offset, and I/Q imbalance at both TX and RX,  $\tilde{z}(t) = z(t) + n(t)$ , as expected.

When noise is present in the observation, its distribution will be important in the construction of good estimators. Here, we only consider the effects of background noise injected at the receiver's antenna. For this, we consider the addition of temporally white, zero-mean, circularly symmetric Gaussian noise  $w(t)$  modulated to the receiver's passband,  $n(t) = \text{Re} \{w(t)e^{j\omega_R t}\}$ . To determine the distribution of the baseband noise due to RX imbalance, we begin with (52), set  $h(t) = \delta(t)$ ,  $a_T = \theta_T = 0$ ,  $z(t) = w(t)$ ,  $r(t) = 1$  and replace  $z_R(t)$  by the baseband noise component  $\tilde{w}(t)$ . In this case,  $k_2 = k_4 = 0$ , and

$$(27) \quad \tilde{w}(t) = \frac{1}{2} [w(t)(1 + e^{-j\theta_R}) + \gamma \star w(t)e^{-j\theta_R} + w^*(t)(1 - e^{j\theta_R}) - \gamma \star w^*(t)e^{j\theta_R}]$$

$$(28) \quad = \text{Re} \{w(t)\} + j \text{Im} \{w(t)e^{-j\theta_R} + \gamma \star w(t)e^{-j\theta_R}\}.$$

In the absence of frequency dependent imbalance, then  $\tilde{w}(t) = \text{Re} \{w(t)\} + j(1 + a_R) \{ \text{Im} \{w(t)\} \cos\theta_R - \text{Re} \{w(t)\} \sin\theta_R \}$ , which is a temporally white zero-mean Gaussian

process. Further, if  $Var(Re\{w(t)\}) = \frac{1}{2}\sigma^2$ , then  $[Re\tilde{w}(t) Im\tilde{w}(t)]^T$  has covariance matrix

$$(29) \quad cov \begin{pmatrix} Re\tilde{w}(t) \\ Im\tilde{w}(t) \end{pmatrix} = \sigma^2 \begin{bmatrix} 1 & (1+a_R)\sin\theta_R \\ (1+a_R)\sin\theta_R & (1+a_R)^2 \end{bmatrix}.$$

Clearly, the noise distribution depends on the RX imbalance parameters. To facilitate the estimation of the parameters, it would be desirable to approximate this covariance matrix by one which is invariant to the unknown parameters. For typical values of RX imbalance ( $0.9dB/4^\circ$ ) then  $a_R = 0.11$ , and the covariance matrix in (29) becomes

$$(30) \quad cov \begin{pmatrix} Re\tilde{w}(t) \\ Im\tilde{w}(t) \end{pmatrix} = \sigma^2 \begin{bmatrix} .5 & 0.04 \\ 0.04 & .61 \end{bmatrix},$$

In the development of estimators, we will approximate the matrix in (30) by the identity. However, it is important to note that in the simulations the true noise distribution will be used.

Using a tap-delay line model for the channel, we now find a matrix representation which will be useful for the next section. We assume that there are  $L + 1$  channel taps  $h_0, \dots, h_L$ , where  $h_l$  is the complex envelope of the impulse response at sample lag  $l$ . Next, we let  $\tilde{\mathbf{z}} = [\tilde{z}(0), \dots, \tilde{z}(N + L - 1)]^T$  denote the vector of received baseband samples,  $\xi_l$  denote the  $l \times 1$  zero vector, and  $\mathbf{z}_l = [\xi_l^T z(0), \dots, z(N - 1), \xi_{L-l}^T]^T$ . Using this notation, we may describe  $\tilde{\mathbf{z}}$  as

$$(31) \quad \tilde{\mathbf{z}} = \mathbf{R}\mathbf{A}\mathbf{p} + \mathbf{R}^*\mathbf{B}\mathbf{q} + \mathbf{n},$$

where  $\mathbf{R} = diag(r(0), \dots, r(N + L - 1))$ ,  $\mathbf{A} = [\mathbf{z}_0, \mathbf{z}_0^*, \mathbf{z}_1, \mathbf{z}_1^*, \dots, \mathbf{z}_L, \mathbf{z}_L^*]$ ,  $\mathbf{B} = [\mathbf{z}_0^*, \mathbf{z}_1^*, \dots, \mathbf{z}_L^*]$ ,  $\mathbf{p} = [h_0k_1, h_0k_2, \dots, h_Lk_1, h_Lk_2]^T$ ,  $\mathbf{q} = [h_0^*k_3, \dots, h_L^*k_3]^T$ , and  $\mathbf{n} = [n(0), \dots, n(N + L - 1)]^T$ .

## 2. Parameter Estimation

**2.1. Phase/Frequency Offset Estimation.** After sampling and quantization, the phase and frequency offsets may be estimated and corrected within the digital domain of the RX. The synchronization factor  $r(t)$  is estimated by cross correlation between the received waveform and known deterministic sequences. In the particular case of IEEE 802.11a, for example, ten replicas of the Short Training Sequence (STS) are transmitted, and the cross correlation outputs are used for coarse, unwrapped, frequency offset acquisition. Additionally, two copies of the Long Training Sequence (LTS) are transmitted, and the cross correlations allow improvements in frequency and phase estimates. In either case, the correlation output for the  $i^{\text{th}}$  transmitted replica of  $z(t)$  at sample time  $t_i$ , may be described by

$$(32) \quad \tilde{R}_i = r(t_i) (k_1 h \star R_{zz}(t_0) + k_2 h \star R_{zz^*}(t_0)) + r^*(t_i) k_3 h^* \star R_{zz^*}(t_0) + v(t_i), \quad i = 0, \dots, T - 1.$$

Here,  $R_{xy}(t)$  denotes the cross correlation between the complex signals  $x(t)$  and  $y(t)$ , and  $v(t)$  describes the colored noise at the correlator output. The cross correlations in (Equation 32) have a common time argument since the time between successive replicas is known at the RX. It is true that  $r(t)$  produces a negligibly relevant phase rotation across the support of  $z(t)$ . In this equation, the combined effect of the I/Q imbalance parameter  $k_2$  and channel response  $h(t)$  is a translation of the circle of rotation of the sequence  $\{\tilde{R}_i\}$  in the complex plane, as seen from the first term of (Equation 32). This is an identical effect as with linear, time-invariant distortion in the absence of I/Q imbalance. Additionally, the effect of the imbalance parameter  $k_3$  is the addition of a counter-rotating component. In this work, traditional estimator is used, as presented in [Hei02] for phase and frequency offset which ignores channel distortion and I/Q imbalance.

In particular, we estimate the frequency offset  $\omega_T - \omega_R$  and phase offset  $\phi_T$  using the least-squares approach applied to the linear phase model  $\arg(\tilde{R}_i) = (\omega_T - \omega_R)t_i + \phi_T + \epsilon(t_i)$ ,  $i =$

$0, \dots, (T - 1)$ , where  $\{\epsilon(t_i)\}$  denotes an uncorrelated, zero-mean wide-sense stationary noise sequence. The performance of this standard estimator is well known in the presence of channel distortion, and it will not be reviewed here. However, Figure 2 shows the resultant error in the noiseless SINR; this shows that while some CFO estimation error is introduced due to I/Q imbalance, the degradation is negligible.

For the remainder of this section, we will ignore estimation errors for the frequency and phase offsets, and define the derotated received baseband vector

$$(33) \quad \hat{\mathbf{z}} = \tilde{\mathbf{R}}^H \tilde{\mathbf{z}} \approx \mathbf{R}^H \tilde{\mathbf{z}} = \mathcal{A} \mathbf{d} + \mathbf{w}.$$

where  $\mathcal{A} = [\mathbf{A} \mid (\mathbf{R}^*)^2 \mathbf{B}]$ ,  $\mathbf{d}^T = [\mathbf{p}^T \mathbf{q}^T]$ , and  $\mathbf{w} = \mathbf{R}^* \mathbf{n}$ . Here, the noise vector has a distribution which does not depend on  $r(t)$ , and it has uncorrelated components. In the numerical results section, the phase and frequency estimation errors will be included in the performance analysis.

**2.2. Estimation of  $a_T, a_R, \theta_T, \theta_R$  and  $\{h_l\}$ .** Since the matrix  $\mathcal{A}$  in (Equation 33) consists of known (or estimated) column vectors, the estimation of  $\mathbf{d}^T = [\mathbf{p}^T \mathbf{q}^T]$  may be achieved by the method of unweighted linear least squares. As the frequency offset decreases in magnitude, however, the condition number of the Gramian  $\mathcal{A}^T \mathcal{A}$  rises (see Figure 4). The resultant effect on the noiseless SINR is depicted in Figure 5; this shows the SINR degradation due to poor conditioning. This is the low-rank case mentioned earlier. For example, when  $z(t)$  corresponds to the IEEE802.11a STS with  $L=4$ , the condition number exceeds 75 when the phase rotation is less than  $0.1^\circ$  during the STS duration (frequency offset magnitude of  $0.15 \text{ ppm}$  at  $5.8 \text{ GHz}$ ). When the frequency instabilities of TX and RX are independent, uniform random variables in the interval  $[-40, +40] \text{ ppm}$ , then this occurs with a probability not greater than 1%. Below, we will first present the algorithm in the case when the condition number of the Gramian is sufficiently small. Then, we will consider the situation when the condition number is high.

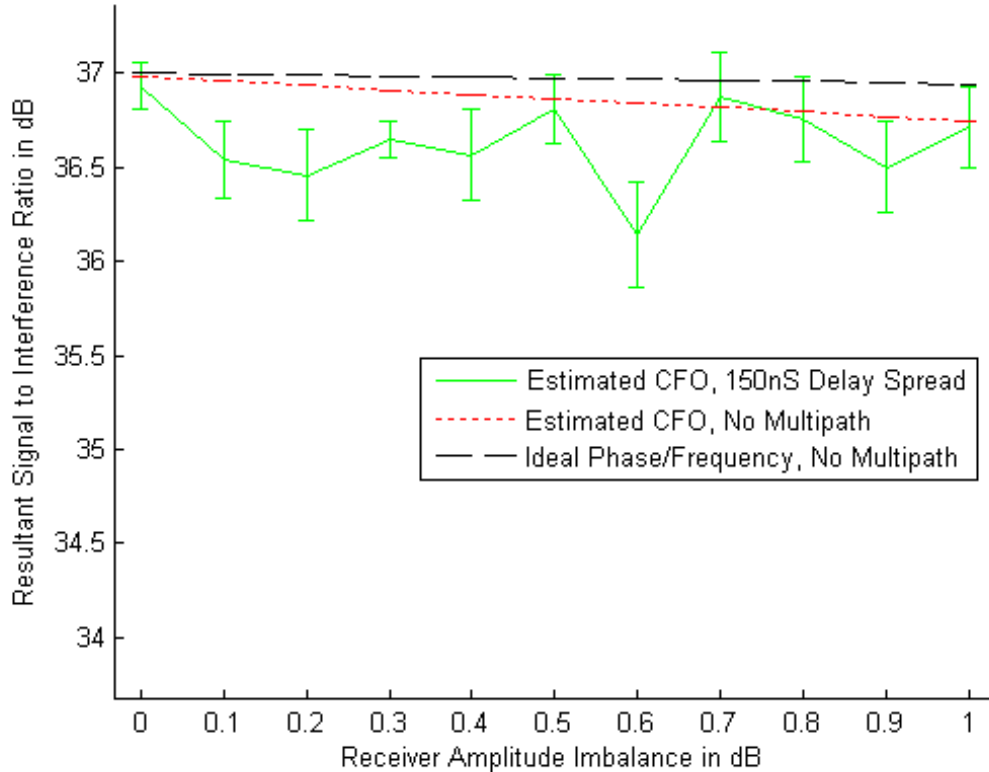


FIGURE 2. The resultant signal to interference ratio (in the absence of noise) for the proposed algorithm is plotted as the RX amplitude imbalance is varied. Here, the frequency offset is 150 kHz, ten packets are simulated per amplitude imbalance value, and three scenarios are demonstrated: 1) basic estimation without multipath, 2) basic estimation with 150 ns of delay spread, and 3) ideal CFO estimation. It is demonstrated that I/Q imbalance has little effect of phase/frequency offset (CFO) estimation for the 802.11a scenario.

The estimators for  $a_T$ ,  $a_R$ ,  $\theta_T$ , and  $\theta_R$  follow from the estimator  $\tilde{\mathbf{d}} = [\tilde{\mathbf{p}}^T \tilde{\mathbf{q}}^T]^T$  and two facts. The first fact, shown by (Equation 34), is that the variable  $c_T = k_2/k_1$  depends only on the TX imbalance parameters. Estimators for  $\theta_T, a_T$  could follow directly from an estimate of  $c_T$ ,  $\tilde{c}_T$  as

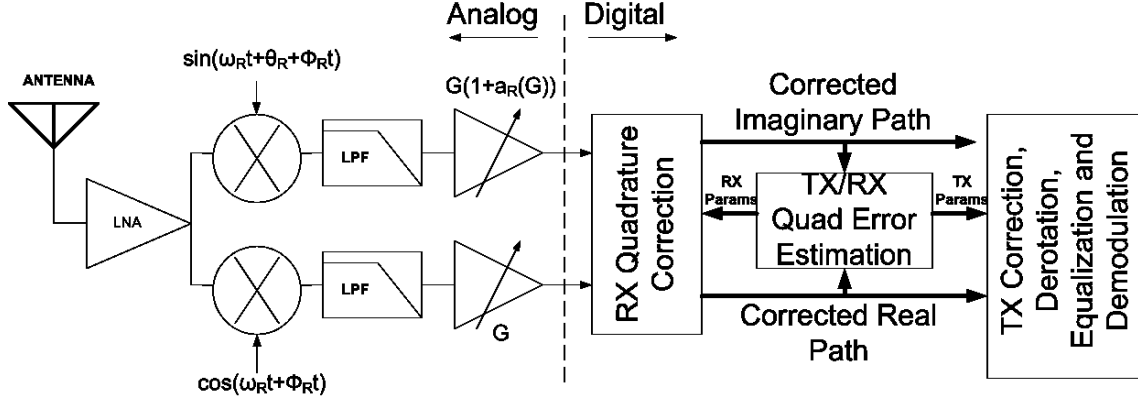


FIGURE 3. The system model for the implementation of the packet switched TX/RX I/Q Imbalance estimation and correction algorithm. The RX correction is placed in-line with the digital baseband signal path such that the subsequent estimation and demodulation algorithms see diminished error after the first full-rank packet is received.

$$(34) \quad \begin{aligned} \tilde{\theta}_T &= \arg \left( \frac{1 - \tilde{c}_T}{\tilde{c}_T + 1} \right), \\ \tilde{a}_T &= \left( \frac{1 - \tilde{c}_T}{\tilde{c}_T + 1} \right) e^{-j\tilde{\theta}_T} - 1. \end{aligned}$$

The estimate  $\tilde{c}_T$  follows from the components of  $\tilde{\mathbf{p}}$  as

$$(35) \quad \begin{aligned} \tilde{c}_T &= \left[ \frac{1}{S} \sum_{l=0}^L \widetilde{h_l k_2} \left( \widetilde{h_l k_1}^* \right) \right], \\ S &= \sum_{l=0}^L |\widetilde{h_l k_1}|^2. \end{aligned}$$

As shown in (Equation 35), the estimate for  $c_T$  is a weighted average of components of  $\tilde{\mathbf{p}}$ . The second fact follows from (Equation 25) that  $c_R = k_3/k_1^*$  provides an expression only in the RX imbalance  $h$  parameters. Setting  $\tilde{c}_R = \left[ \frac{1}{S} \sum_{l=0}^L \widetilde{h_l^* k_3} \left( \widetilde{h_l k_1} \right) \right]$ , which is determined from the estimates of the vectors  $\mathbf{q}$  and  $\mathbf{p}$ , we have

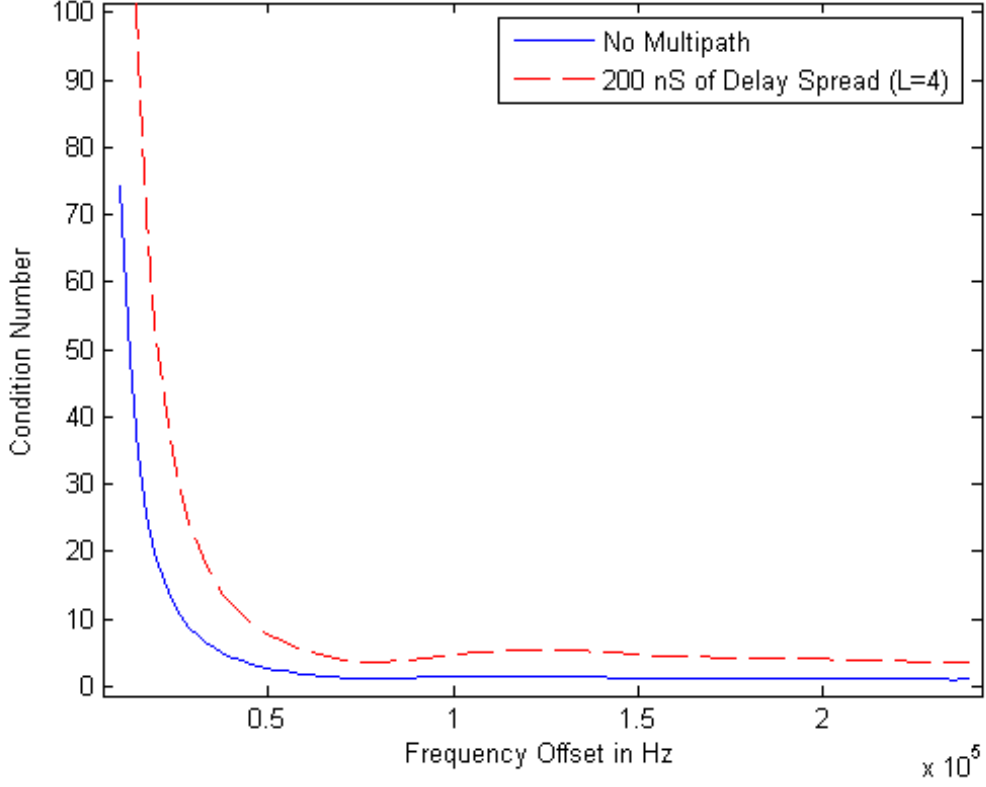


FIGURE 4. As the phase/frequency error between the TX and the RX approach zeros, the Grammian  $\mathbf{A}^T \mathbf{A}$  becomes badly conditioned and this problem is no longer full rank. The condition number for the Grammian (using the LTS) non-multipath and the L=4 (200 nS delay spread) case is plotted versus the frequency offset. Note: 240 KHz is equivalent to +40 ppm at 5.8 GHz.

$$(36) \quad \begin{aligned} \tilde{\theta}_R &= \arg \left( \frac{1 - \tilde{c}_R}{\tilde{c}_R + 1} \right), \\ \tilde{a}_R &= \left( \frac{1 - \tilde{c}_R}{\tilde{c}_R + 1} \right) e^{-j\tilde{\theta}_R} - 1. \end{aligned}$$

Estimation of the channel coefficients follows from the estimation of the IQ imbalance parameters and the product vector  $\tilde{\mathbf{p}}$ . By defining the estimator  $\tilde{k}_1 = \frac{1}{4}(1 + (1 + \tilde{a}_R)e^{-j\tilde{\theta}_R})(1 + (1 + \tilde{a}_T)e^{j\tilde{\theta}_T})$ , the channel coefficients may be estimated by  $\tilde{h}_l = \widetilde{h}_l \tilde{k}_1 / \tilde{k}_1$ ,  $l = 0, 1, \dots, L$ .

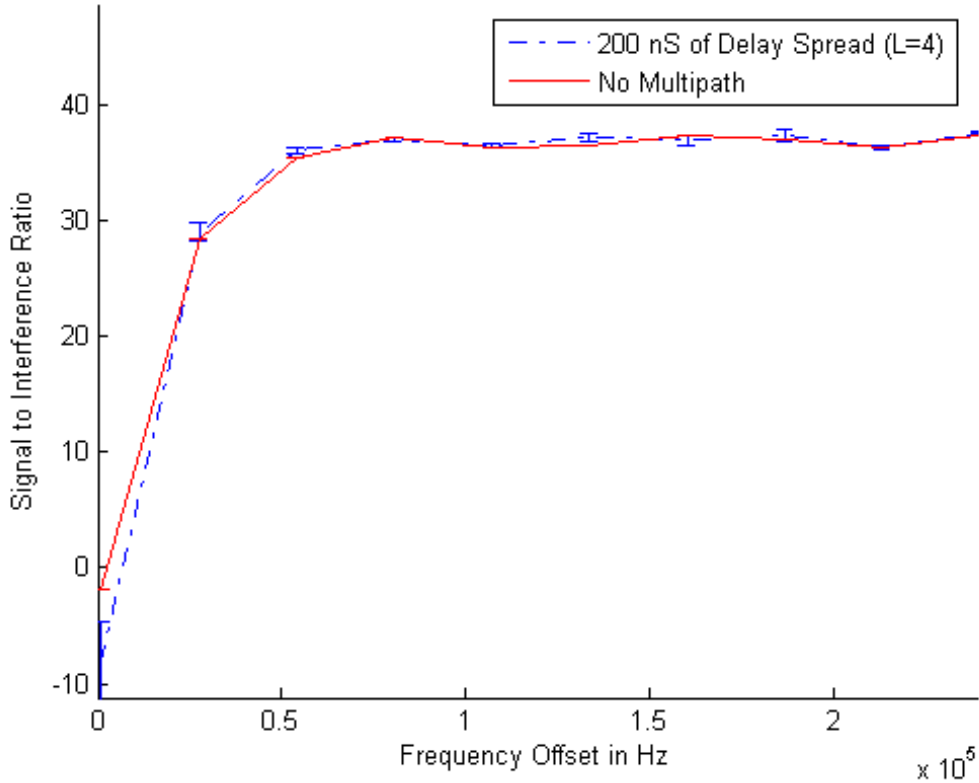


FIGURE 5. The signal to interference ratio (in the absence of noise) for the proposed algorithm is plotted versus frequency offset in the presence of I/Q imbalance (TX Error of  $.5\text{dB}/-5^\circ$ , RX Error of  $.9\text{dB}/5^\circ$ , and Delay Spread of 200ns)

In the case when the Grammian has a high condition number, we propose to use existing estimates of the RX imbalance parameters from previous OFDM frames at similar gain settings. The location of the RX I/Q imbalance correction algorithm, as shown in Figure 3 facilitates this technique where historical RX correction results continue to be applied to the incoming waveform— this is particularly helpful for both the low-rank situation and further reduces the contribution of CFO estimation error since the remainder of the algorithm is exposed to a waveform that is already corrected for RX I/Q imbalance.

These estimates may be used to correct the RX-induced error, producing a new observation. In all subsequent calculations, we propose to set the equivalent RX parameters  $a_R, \theta_R$

to 1 and 0, respectively. As shown by (Equation 25), the parameter  $k_3$  is set to zero, and from (Equation 31) the vector  $\mathbf{q}$  is the zero vector. Accordingly, we set  $\mathcal{A} = \mathbf{A}$  in (Equation 31) and estimate only the vector  $\mathbf{p}$ . In this case,  $\mathcal{A}$  has full column rank, and the least squares solution for  $\mathbf{p}$  is well defined. Estimation of the TX imbalance parameters and channel parameters proceeds as above.

### 3. Compensation Algorithm

The received signal,  $z_R(t)$ , is corrected in reverse order as the distortions occurred, as described in the following steps:

- 1) RX I/Q imbalance is corrected, and the phase/frequency offset is derotated:

$$(37) \quad z_C(\widehat{t_i})r^*(t_i) = \widehat{r}^*(t_i) \left( \text{Re}(\tilde{z}(t_i)) + \text{Im}(\tilde{z}(t_i))\tan(\tilde{\theta}_R) + j\text{Im}\{\tilde{z}(t_i)\} \left( \cos(\tilde{\theta}_R)\tilde{a}_R \right)^{-1} \right)$$

- 2) The channel distortion is mitigated linearly in the frequency domain ( symbol ./ denotes component-wise division):

$$(38) \quad FFT \left( z_T(\widehat{t})r^*(t) \right) = FFT \left( \left\{ z_C(\widehat{t_i})r^*(t_i) \right\} \right) ./ FFT([\tilde{h}_0 \dots \tilde{h}_L \ 0_{N-L}]).$$

- 4) The derotated TX I/Q imbalance is corrected in the frequency domain:

$$(39) \quad FFT \left( \widehat{z}(t) \right) = \sum_{r=1}^{N-1} \left( (1 + (1 + \tilde{a}_T)e^{j\tilde{\theta}_T}) \right)^{-1} \left[ \widehat{Z}_{T0}(b) - \left( (1 - (1 + \tilde{a}_T)e^{j\tilde{\theta}_T}) \widehat{Z}^*(L - b) \right) \right],$$

where  $\widehat{Z}_{T0}(b)$  represents the FFT of  $z_T(\widehat{t})r^*(t)$  at spectral bin  $b$ . In the following section this procedure is applied to simulated signals, and compared to previously proposed solutions.

### 4. Numerical Results

Fully compliant 1000 byte 54 Mbps IEEE802.11a packets are generated and then passed through the TX, channel, and RX models as described in Section 2. The compensation algorithm presented in Section 3, and those in [Xin05] and [Tar07] are applied to the

demodulated waveform, where the corrected result is then compared to the ideal transmitted waveform. The Rayleigh channel model is implemented as an FIR whose complex coefficients are exponentially scaled complex Gaussian random variables. With the exception of [Tar07], which incorporates the channel estimation coefficients within the algorithm, equalization is performed in the frequency domain according to [Hei02]. We also consider a genie-aided approach to the algorithm in [Tar07], where the true channel parameters are used, rather than their estimates. The I/Q Imbalance correction parameters are estimated and corrected separately for each packet based only on the linear least squares estimator of the two symbols of the 802.11a LTS (though the estimation accuracy would improve if memory were applied). It is important to note that in order to compare our algorithm fairly to algorithms unintended for packet-switched scenarios, the channel and TX parameters are static for all packets in the sequence.

First we consider the case of mild TX (TX) imbalance. For these simulations, the delay spread was set to a typical value of 150 ns, and a moderate frequency offset of 15 ppm (90 KHz) was chosen as well as very mild TX impairments (.1dB for amplitude imbalance and  $-1^\circ$  of phase imbalance). A moderate RX imbalance (amplitude imbalance of .9dB and a phase imbalance of  $4^\circ$ ) was chosen, and the signal-to-noise ratio (SNR) is varied over a range of 15dB to 35dB. For comparison purposes, it is useful to note that a signal-to-noise-plus-interference ratio (SINR) of approximately 20 dB is required to achieve the 802.11a-specified packet error rate of 10%. Under ideal circumstances (no signal distortion of any kind), the SINR is equal to the SNR. Figure 6 compares the results of four approaches: [Xin05] (intended for situations where the TX exhibits no impairment), [Tar07], the proposed algorithm, and no attempt at compensation. Error bars at each data point span  $\pm 1$  standard deviation of simulated realizations. It is shown that that even very small TX I/Q imbalance (similar in magnitude to that of a hardware-calibrated TX) causes a significant SINR degradation. The interpretation of this result is that TX I/Q imbalance should not be ignored, even at very low levels.

Figure 7 shows a comparison of the ideal case with the same four approaches as in Figure 6 with more severe TX impairment ( $.4\text{dB}/-5^\circ$ ). The other simulation parameters are unchanged. Again, the error bars span  $\pm 1$  standard deviation of simulated realizations. This particular result demonstrates that even under severe circumstances, it is still possible to compensate for I/Q imbalance, channel distortion, and frequency offset. Here, at each SNR, there is approximately a 2.5 dB gap between the SINR of our algorithm and the ideal result. This constant error offset is attributed in part to the low complexity frequency-domain OFDM equalization technique .

Figure 8 then shows a comparison of the four approaches, under the same conditions as Figure 7, but with zero frequency offset. This simulation assumes that, at some point in the past, a full rank packet has been received, and our algorithm defaults to the high-condition-number approach, where the previously estimated RX parameters are applied, the data matrix  $A$  is used, and only vector  $\mathbf{p}$  is estimated. In the simulation, the previously estimated RX parameters are uniformly selected within one standard deviation of the true parameters, where the standard deviation is chosen from Figure 7. It is shown in Figure 8 that the proposed algorithm is an effective for packet-switched direct-conversion transceivers in which each packet has was sent by the same TX. When successive packets come from different TXs, the displayed performance of the proposed algorithm is preserved.

## 5. Conclusions

This chapter describes a novel direct conversion I/Q Imbalance correction algorithm intended for packet switching environments, where each of the following impairments must be quickly estimated and corrected: TX I/Q imbalance, channel distortion, frequency offset, and RX I/Q imbalance. A deployable algorithm, developed within the framework of IEEE802.11a OFDM modulation, is presented and compared to existing approaches on simulated data. This algorithm, which operates within the framework of the existing standard, is implemented completely within the baseband signal processor at the RX. A partitioned

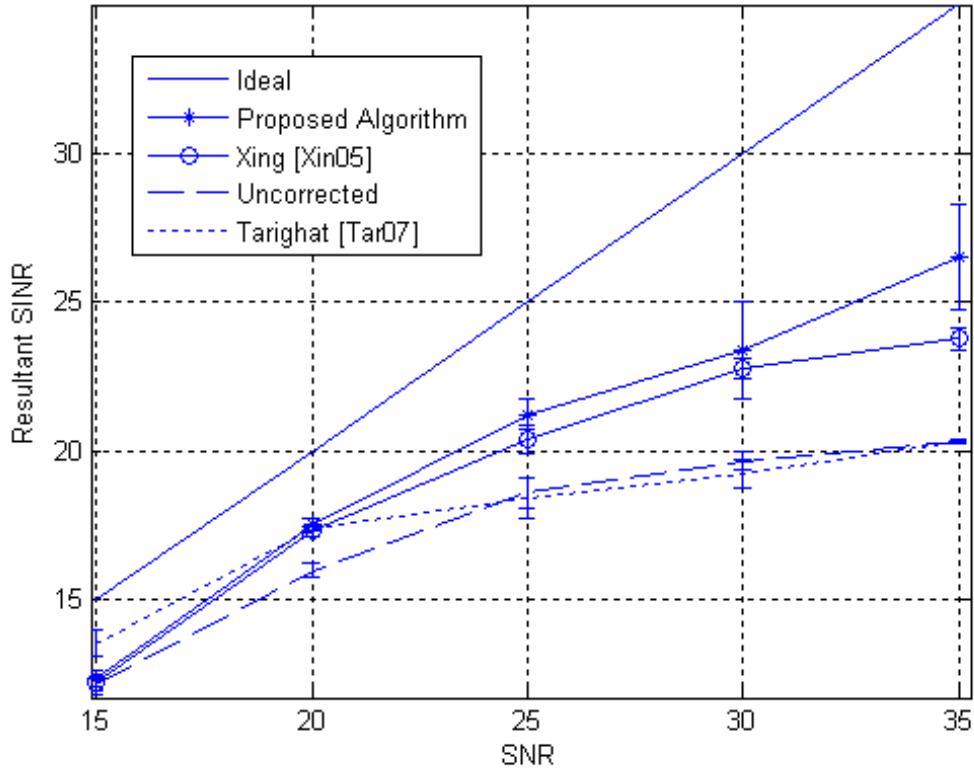


FIGURE 6. Comparison of algorithm performance with a 15 ppm Frequency Offset (90 KHz) and modest I/Q imbalance (TX Error of  $.1\text{dB}/-1^\circ$ , RX Error of  $.9\text{dB}/4^\circ$ , and Delay Spread of 150ns).

system state memory algorithm that mitigates the effects of the occasional low-rank scenario (approximately 1% of 802.11a packets are low-rank) is proposed, which solves this problem. Simulation results have shown that under typical values of link impairments and signal strengths, the proposed algorithm approaches the ideal SINR to within 2.5dB.

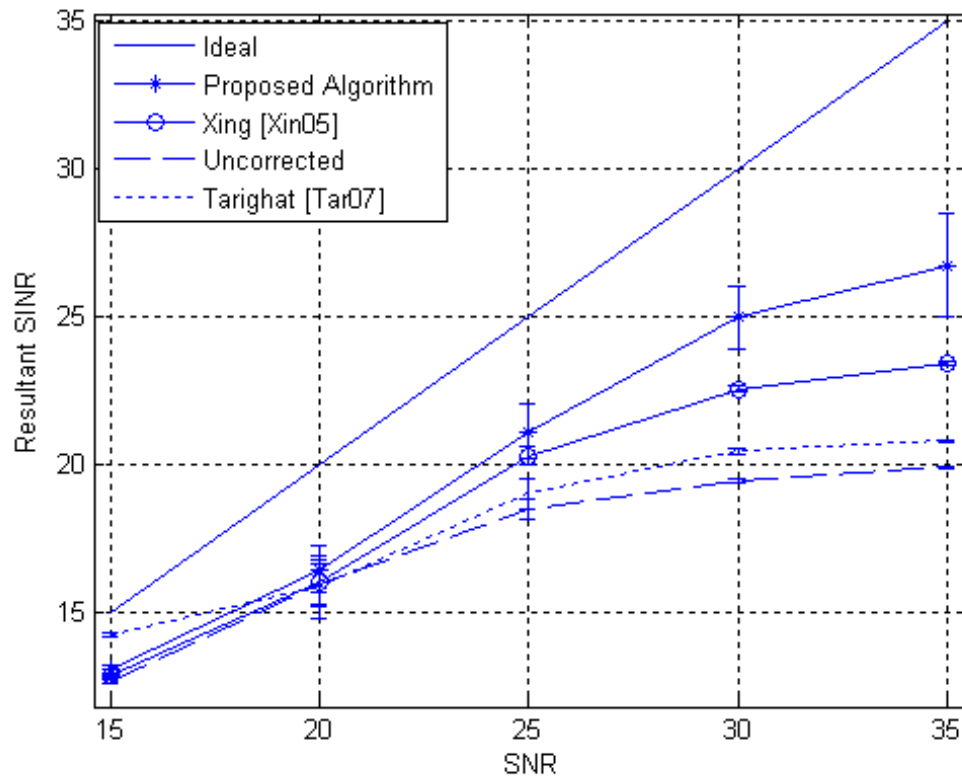


FIGURE 7. Algorithm performance with a 15 ppm Frequency Offset (90 KHz) and severe I/Q imbalance (TX Error of  $.5\text{dB}/-5^\circ$ , RX Error of  $.9\text{dB}/4^\circ$ , and Delay Spread of 150nS).

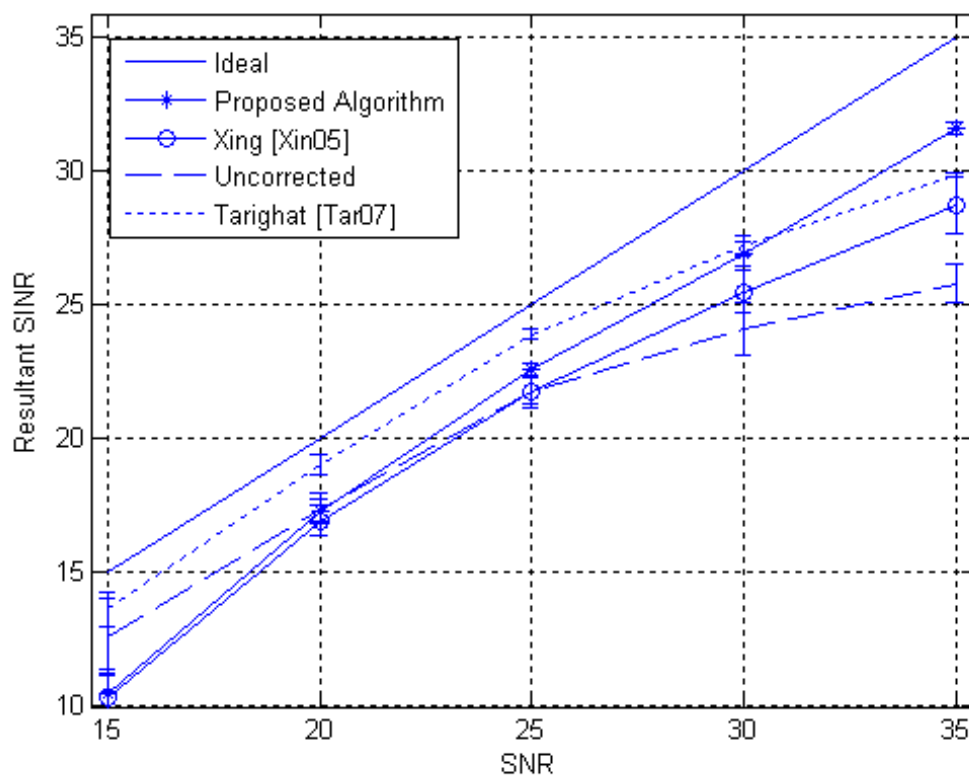


FIGURE 8. Comparison of algorithm performance with a 0 ppm (Synchronous) Frequency Offset, TX Error of  $.5\text{dB}/-5^\circ$ , RX Error of  $.9\text{dB}/4^\circ$ , and Delay Spread of 150ns, using a historical RX Estimate

## CHAPTER 3

# A Non-Linear Constrained Least Squares Approach

### 1. Introduction

The algorithmic capabilities of modern digital integrated circuit technology, often characterized by “Moore’s Law”, continues to grow at an exponential rate. High volume semiconductor processes such as CMOS (Complimentary Metal Oxide Semiconductor) and related technologies offer an extremely inexpensive means (when produced in large volumes) of integrating a large number of transistors and other circuit elements onto a single substrate. Unfortunately, there exists no such parallel of “Moore’s Law” for analog and radio communications circuits, regardless of the attractive cost incentive and integration potential of modern integrated circuit processes. Furthermore, effective monolithic integration requires significant architectural modification, while performance is often degraded from that of their less integrated counterparts.

Many modern consumer communications systems, including broadband wireless, are comprised of direct conversion radio architectures in combination with OFDM (Orthogonal Frequency Domain Multiplexing) modulation. These systems utilize high-order constellations (up to 64-QAM) where even a small degradation in signal fidelity impacts the communications performance. In a previous work we detailed a deployable algorithm that estimates and corrects such an OFDM waveform under practical packet-switching scenarios[**Fei08**]. In that work, the model is comprehensive in that it accounts for phase/frequency offset, frequency independent TX and RX I/Q imbalance, and dispersive multipath, all on a packet-by-packet basis. However, the solution was developed with a focus of low computational effort. The

current work considers an enhanced correction scheme that, at the expense of more algorithmic processing power, further improves system performance.

There exists a large body of literature on the subject of I/Q imbalance, with substantial works that focus on OFDM in the presence of dispersive multipath. Some of these publications (such as [Xin05, Tub03, Val01, Bar07, Val05, Val05a, Par07]) focus on communications systems where only the RX suffers from I/Q imbalance (commercial subscriber-quality basestation TXs typically exhibit perfect quadrature). [Hai08, Hai07] extends the work of [Xin05] by proposing a solution to the low-rank problem that develops when the Carrier Frequency Offset (CFO) is very small. [Ryk08] analyzes the equalization problem for this scenario while [Zou08] considers the effects under the joint TX/RX scenario in the context of space-time coding. Other publications also consider both TX and RX I/Q imbalance, but model frequency-synchronous systems with zero CFO([Tar07, Sch06]) .

Work [Tan07] considers the asynchronous case where both the TX and RX suffer I/Q imbalance in the presence of multipath (without consideration for the low-rank case), but requires relatively static channel and TX I/Q imbalance parameters. IEEE802.11a [IEE99] operation (two equalizer training symbols per packet) provide two opportunities to update the specified LMS algorithm per packet. As the channel and TX I/Q imbalance parameters can be different for each received packet, in a multiuser environment , these parameters would change far faster than such a loop could converge.

Work [Tan07] also considers a frequency dependent I/Q imbalance while this work considers frequency independent model; this difference in modeling is primarily attributed to differences in the assumptions concerning the I-channel and quadrature (Q)-channel analog filters. Single-chip direct conversion design efforts such as those presented in [Chi06, Zha05] utilize self calibrating analog filters (presumably using a technique that adjusts the filters according to the system clock reference) while no similarly effective circuit-based

I/Q imbalance correction technique exists. Although there still exists residual frequency-dependent error, this phenomenon is considered a second-order effect in WLAN, but quite important for UWB where the channel bandwidth is approximately 30 times larger.

The multiuser scenario is particularly important for unlicensed networks such as IEEE802.11a Wireless LAN because these devices receive packets from multiple TXs, some of which are co-channel users. The network adapter must decode every packet, since this is only way to determine the intended recipient. As each TX has unique I/Q imbalance parameters and relative phase/frequency offset, the estimation results must be partitioned such that the phase/frequency and TX I/Q imbalance parameters are discernible from one another. It is of further importance to note that receive I/Q imbalance is a function of RX gain (this is because a direct conversion RX uses separate variable-gain paths for the I and Q channels)—each received packet, even from the same TX, is likely to result in a different RX gain settings. The multiuser scenario requires each packet to be considered separately and it is only possible to maintain a memory-based correction for RX parameters.

This proposed algorithm, as with its low-complexity predecessor presented in [Fei08], operates within the framework of any OFDM standard. In this venue, only a training sequence is required without the need for any special provisions or modifications. Using only the provided channel estimation sequence, this algorithm estimates both the TX and RX I/Q imbalance parameters in the presence of a phase/frequency error and dispersive multipath. Most importantly, this technique relies solely upon the preamble interval of the incoming packet, even when the packet emanates from a unique TX with phase/frequency and I/Q imbalance parameters in which there is no historical knowledge. This algorithm is executed until a sufficient I/Q imbalance vs. gain correction function is built within the RX, then reduces its rank since only TX I/Q imbalance remains. Upon successful reception of only a few packets, the estimation of the RX's I/Q imbalance parameters converges and hence there exists minimal effect upon the in-line CFO estimation algorithm.

First, the system model from the previous work is briefly presented the reformulated in way that aids Constrained Least Squares Estimation (CLSE). Next, a cost function is given and an interactive form of the Newton-Raphson approach is formulated. An improved equalization technique, whose parameters are found as part of this technique, is presented. In the simulation results section, the performance is of this algorithm, in comparison with several variants as well as two non packet-switching works [Tar07, Xin05] are presented in a static simulation environment (where the TX and CFO parameters are static). Finally, this algorithm is presented under the intended multiuser scenario, in comparison with another work, [Tan07], that also considers TX and RX I/Q imbalance and CFO but was not intended for the dynamic packet-switching environment.

## 2. System model

In this section we present a brief recap of the system model from [Fei08], then present a new formulation. The complex envelope of the undistorted transmitted signal,  $z(t)$ , is related to the noiseless complex baseband received signal after down-converting  $z_R(t)$ . As in [Fei08], we continue to rely upon a known training sequence (the Long Training Sequence, or LTS in the case of 802.11a) to estimate all of the necessary distortion parameters at the RX. Setting the RX's I-branch as the phase reference, and we define the complex envelope  $c(t)$  of a passband signal  $x(t)$  with respect to the RX's In-phase branch,  $x(t) = \text{Re}(c(t)e^{j\omega_R t})$ . Here,  $\omega_R$  is the radian carrier frequency of the RX.

Variables  $a_T, \theta_T$  (resp.  $a_R, \theta_R$ ) denotes the relative amplitude and phase imbalance of the TX's (resp. RX) quadrature branch . The function  $r(t) = e^{j(\omega_T - \omega_R)t + j\phi_T}$  accounts for the instantaneous phase offsets between the TX's and RX's I-branches. Quantity  $h(t)$  denotes the complex envelope of the impulse response, which is assumed to remain constant for the duration of the packet.

The resultant signal at the RX,  $z_R(t)$ , is then found to be:

$$(40) \quad \begin{aligned} z_R(t) = & r(t)\alpha\beta h \star z(t) + r(t)\alpha(1 - \beta)h \star z^*(t) + \\ & r^*(t)(1 - \alpha^*)\beta^* h^* \star z^*(t) + r^*(t)(1 - \alpha^*)(1 - \beta^*)h^* \star z(t), \end{aligned}$$

where  $\alpha = \frac{1}{2}(1 + (1 + a_R)e^{-j\theta_R})$ , and  $\beta = \frac{1}{2}(1 + (1 + a_T)e^{j\theta_T})$ . Finally, we express the system model in matrix form as

$$(41) \quad \hat{\underline{Z}} = \mathbf{M}\underline{b} + \underline{n}$$

such that

$$(42) \quad \mathbf{M} = \begin{bmatrix} (\alpha\beta\mathbf{R} + (1 - \beta^*)(1 - \alpha^*)\mathbf{R}^*)\mathbf{Z} + (\alpha(1 - \beta)\mathbf{R} + (1 - \beta^*)\alpha^*\mathbf{R}^*)\mathbf{Z}^* \\ (\alpha\beta\mathbf{R} - (1 - \beta^*)(1 - \alpha^*)\mathbf{R}^*)j\mathbf{Z} + (\alpha(1 - \beta)\mathbf{R} - (1 - \beta^*)\alpha^*\mathbf{R}^*)j\mathbf{Z}^* \end{bmatrix},$$

$\underline{b} = \begin{bmatrix} Re\{\underline{h}^T\} & Im\{\underline{h}^T\} \end{bmatrix}^T$  and  $\underline{h} = [h(0), h(1) \dots h(L-1)]^T$ . Here,  $\mathbf{Z}$  is the known  $N+L$  by  $L$  Toeplitz matrix whose first column is  $[z(0), z(1), \dots, z(N+L-1)]^T$  and whose first row is  $[z(0), 0 \dots 0]$ ,  $N$  is the length of the transmitted sequence,  $L$  is the number of delay taps of the multipath channel, and  $\mathbf{R}$  is the  $N$  by  $N$  diagonal matrix  $diag(r(0), r(1), \dots, r(N-1))$ . Sample times of the sequence are assumed to be uniformly spaced as  $0, 1, \dots, N+L$ .

### 3. Parameter Estimation

In this section, we describe the estimation approach.

This technique uses a CLSE to determine estimates  $\hat{\alpha}$  and  $\hat{\beta}$ , while  $b$  (a fixed parameter) and  $\mathbf{R}$  are found using the Linear Least Squares Estimator (LLSE) technique described in [Fei08]. Note that the estimation of RX ( $\alpha$ ) and TX ( $\beta$ ) I/Q imbalance parameters are kept separate, which enables a refinement of the initial guess for the RX's I/Q imbalance

parameter as more packets are received. As the RX's I/Q imbalance parameter is estimated more accurately as the packets arrive, the CFO estimation algorithm operates on a waveform with only a decreasing residual I/Q imbalance. For the first few packets, the estimate for  $\mathbf{R}$  can be improved by using techniques presented in [Fou02, Yan07, Yan04, Tub03].

A cost function, which is the mean squared difference between the received training sequence and the forward distortion function, is found according to:

$$(43) \quad J = \left\| \hat{\underline{Z}} - \mathbf{M}\underline{b} \right\|^2$$

Estimates  $\hat{\alpha}$  and  $\hat{\beta}$  are then found by minimizing this cost function via both the Newton-Raphson algorithm and a serial single-dimension parameter search. In the latter case, a scalar optimization is performed for each component of the estimation vector separately. In both cases the initial I/Q imbalance parameter estimates follow from the LLSE algorithm described in [Fei08]. Next we describe the Newton-Raphson approach to minimize the cost function. The iterative form for this algorithm is:

$$(44) \quad \underline{V}_{i+1} = \underline{V}_i - \mathbf{H}^{-1} \underline{\nabla} J$$

where  $\underline{V}_i$  is the  $i^{th}$  iteration,  $i = 0, 1, \dots$  of the 1x4 estimation vector  $[ \text{Re}\{\hat{\alpha}\} \quad \text{Im}\{\hat{\alpha}\} \quad \text{Re}\{\hat{\beta}\} \quad \text{Im}\{\hat{\beta}\} ]^T$ ,  $i$  is the loop iteration number,  $\mathbf{H}$  is the Hessian Matrix of  $J$  and  $\underline{\nabla} J$  and refers to the gradient of  $J$ , both with respect to  $\underline{V}_i$ . Since the partial derivative of  $J$ , with respect to any real parameter  $x$  is given by :

$$(45) \quad \frac{\partial J}{\partial x} = -2 \text{Re} \left\{ \left( \frac{\partial \mathbf{M}\underline{b}}{\partial x} \right)^H \left( \hat{\underline{Z}} - \mathbf{M}\underline{b} \right) \right\},$$

the gradient of  $J$  with respect to  $\mathbf{V}$  is:

$$(46) \quad \underline{\nabla J} = -2Re\left\{ \left[ \begin{array}{c} \left( \left( \frac{\partial \mathbf{M}}{\partial Re\{\alpha\}} \right)^H (\tilde{\underline{Z}} - \mathbf{M}\underline{b}) \right), \\ \left( \left( \frac{\partial \mathbf{M}}{\partial Im\{\alpha\}} \right)^H (\tilde{\underline{Z}} - \mathbf{M}\underline{b}) \right), \\ \left( \left( \frac{\partial \mathbf{M}}{\partial Re\{\beta\}} \right)^H (\tilde{\underline{Z}} - \mathbf{M}\underline{b}) \right), \\ \left( \left( \frac{\partial \mathbf{M}}{\partial Im\{\beta\}} \right)^H (\tilde{\underline{Z}} - \mathbf{M}\underline{b}) \right) \end{array} \right]^T \right\}$$

$\partial \mathbf{M}\underline{b}/\partial x$  is then found for each parameter:

$$(47) \quad \begin{aligned} \frac{\partial \mathbf{M}}{\partial Re\{\alpha\}} &= \left[ \begin{array}{c} (\hat{\alpha}\mathbf{R} - (1 - \hat{\alpha}^*)\mathbf{R}^*)\mathbf{Z} + ((1 - \hat{\alpha})\mathbf{R} - \hat{\alpha}\mathbf{R}^*)\mathbf{Z}^* \\ (\hat{\alpha}\mathbf{R} + (1 - \hat{\alpha}^*)\mathbf{R}^*)j\mathbf{Z} + ((1 - \hat{\alpha})\mathbf{R} - \hat{\alpha}\mathbf{R}^*)j\mathbf{Z}^* \end{array} \right], \\ \frac{\partial \mathbf{M}}{\partial Im\{\alpha\}} &= \left[ \begin{array}{c} (j\hat{\alpha}\mathbf{R} + j(1 - \hat{\alpha}^*)\mathbf{R}^*)\mathbf{Z} + (j(1 - \hat{\alpha})\mathbf{R} + j\hat{\alpha}\mathbf{R}^*)\mathbf{Z}^* \\ (j\hat{\alpha}\mathbf{R} - j(1 - \hat{\alpha}^*)\mathbf{R}^*)j\mathbf{Z} + (j(1 - \hat{\alpha})\mathbf{R} - j\hat{\alpha}\mathbf{R}^*)j\mathbf{Z}^* \end{array} \right] \\ \frac{\partial \mathbf{M}}{\partial Re\{\beta\}} &= \left[ \begin{array}{c} (\hat{\beta}\mathbf{R} - (1 - \hat{\beta}^*)\mathbf{R}^*)\mathbf{Z} + ((1 - \hat{\beta})\mathbf{R} - \hat{\beta}\mathbf{R}^*)\mathbf{Z}^* \\ (\hat{\beta}\mathbf{R} + (1 - \hat{\beta}^*)\mathbf{R}^*)j\mathbf{Z} + ((1 - \hat{\beta})\mathbf{R} - \hat{\beta}\mathbf{R}^*)j\mathbf{Z}^* \end{array} \right], \sim \text{and} \\ \frac{\partial \mathbf{M}}{\partial Im\{\beta\}} &= \left[ \begin{array}{c} (j\hat{\beta}\mathbf{R} + j(1 - \hat{\beta}^*)\mathbf{R}^*)\mathbf{Z} + (j(1 - \hat{\beta})\mathbf{R} + j\hat{\beta}\mathbf{R}^*)\mathbf{Z}^* \\ (j\hat{\beta}\mathbf{R} - j(1 - \hat{\beta}^*)\mathbf{R}^*)j\mathbf{Z} + (j(1 - \hat{\beta})\mathbf{R} - j\hat{\beta}\mathbf{R}^*)j\mathbf{Z}^* \end{array} \right]. \end{aligned}$$

The Hessian matrix may be developed similarly, following from the partial derivatives in Equation 47. The  $(i, j)^{th}$  component of the Hessian matrix  $\mathbf{H}$  is the second partial derivative of  $J$ , with respect to the  $i^{th}$  and  $j^{th}$  components of the estimation vector (here  $x$  and  $y$  respectively)

$$(48) \quad \mathbf{H}_{ij} = \frac{\partial^2 J}{\partial x \partial y} = -2Re\left\{ \left( \frac{\partial^2 \mathbf{M}\underline{b}}{\partial x \partial y} \right)^H (\tilde{\underline{Z}} - \mathbf{M}\underline{b}) - \left( \frac{\partial \mathbf{M}\underline{b}}{\partial x} \right)^H \left( \frac{\partial \mathbf{M}\underline{b}}{\partial y} \right) \right\}.$$

The Hessian matrix may be populated using the following expressions for the partial derivatives for the matrix  $\mathbf{M}$ ,

$$(49) \quad \frac{\partial^2 \mathbf{M}}{\partial x^2} = 0$$

and:

$$(50) \quad \begin{aligned} \frac{\partial^2 \mathbf{M}}{\partial \text{Re}\{\alpha\} \partial \text{Re}\{\beta\}} &= \begin{bmatrix} (\mathbf{R} + \mathbf{R}^*)\mathbf{Z} - (\mathbf{R} + \mathbf{R}^*)\mathbf{Z}^* \\ (\mathbf{R} - \mathbf{R}^*)j\mathbf{Z} + (-\mathbf{R} + \mathbf{R}^*)j\mathbf{Z}^* \end{bmatrix}, \\ \frac{\partial^2 \mathbf{M}}{\partial \text{Re}\{\alpha\} \partial \text{Im}\{\beta\}} &= \begin{bmatrix} (j\mathbf{R} - j\mathbf{R}^*)\mathbf{Z} - (-j\mathbf{R} + j\mathbf{R}^*)\mathbf{Z}^* \\ (j\mathbf{R} + j\mathbf{R}^*)j\mathbf{Z} - (-j\mathbf{R} - j\mathbf{R}^*)j\mathbf{Z}^* \end{bmatrix}, \\ \frac{\partial^2 \mathbf{M}}{\partial \text{Im}\{\alpha\} \partial \text{Re}\{\beta\}} &= \begin{bmatrix} (j\mathbf{R} - j\mathbf{R}^*)\mathbf{Z} - (-j\mathbf{R} + j\mathbf{R}^*)\mathbf{Z}^* \\ (j\mathbf{R} + j\mathbf{R}^*)j\mathbf{Z} - (-j\mathbf{R} - j\mathbf{R}^*)j\mathbf{Z}^* \end{bmatrix}, \\ \frac{\partial^2 \mathbf{M}}{\partial \text{Im}\{\alpha\} \partial \text{Im}\{\beta\}} &= \begin{bmatrix} (-\mathbf{R} - \mathbf{R}^*)\mathbf{Z} - (\mathbf{R} + \mathbf{R}^*)\mathbf{Z}^* \\ (-\mathbf{R} + \mathbf{R}^*)j\mathbf{Z} + (\mathbf{R} - \mathbf{R}^*)j\mathbf{Z}^* \end{bmatrix}. \end{aligned} \quad \sim \text{and}$$

The Newton-Raphson approach begins with an initial estimate  $\underline{V}_0$  obtained from the algorithm described in [Fei08]. The algorithm iterates on the index  $i$  until a maximum iteration is reached, or the fractional change in the norm of the current estimation vector is below a tolerance. For the simulations presented in Section 4, the maximum iteration count was 100 and the tolerance for the fractional error was  $10^{-4}$ .

The serial search method may be concisely described using similar notation to that presented above, although simpler and equivalent descriptions are possible. In this case, let  $k = 1, 2, \dots, 4$  denote the current dimension index,  $i = 0, 1, \dots$  denote the iteration index, and  $\underline{V}_{k,i}$  denote the realization of the estimation vector. The iteration for index  $k$  proceeds as follows

$$\underline{V}_{k,(i+1)} = \underline{V}_{k,i} - \underline{\epsilon} d_k$$

where  $\varepsilon > 0$  denotes the step-size, and  $\underline{d}_k$  is a vector obtained by the gradient vector by setting all but the  $k^{th}$  component to zero. For step  $k = 1$ , the initial value of the estimation vector  $V_{1,0}$  is provided from the method described in [Fei08]. The termination conditions for the  $k^{th}$  component consider a threshold on the fractional change in the norm of the estimation vector as well as a maximum iteration index. For the simulations in Section 4 this threshold was  $10^{-4}$  and the maximum iteration count was 100. If we define the final value for the estimation vector in the  $k \geq 1$  step as  $\underline{V}_{k,\infty}$ , then the  $k + 1^{st}$  step begins with the initialization  $\underline{V}_{(k+1),0} = \underline{V}_{k,\infty}$ .

Relative complexity, based upon Matlab simulation time, is found to be approximately 10% that of the Newton-Raphson approach. In comparison, the baseline LLSE approach, which is implemented in matrix form without the need for loop-type operations, executes in approximately 1% of the time as the Newton Raphson method.

As described in [Hei02], the common low-complexity equalization technique for OFDM is simple frequency-domain correction, where two received LTS symbols are averaged then divided by the known LTS (adapted from [Hei02] p.77). Since this paper focuses on high performance approaches, at the expense of more complexity, we consider a more accurate frequency domain channel estimator that is used in the same fashion. This technique uses the  $h_1 \dots h_L$  estimates from [Fei08], and then estimates the frequency-domain taps as:

$$(51) \quad S(k) = FFT(h_1 \dots h_L, 0_{k-L})$$

where  $k$  is the subcarrier index. All succeeding OFDM symbols are then divided by the frequency-domain channel estimate, exactly as in conventional OFDM frequency domain equalization.

#### 4. Simulation Results

This simulation emulates a direction conversion TX that sends individual 802.11a standard compliant packets to an asynchronous direct conversion RX through a dispersive multipath channel. The Signal to Noise Ratio (SNR) is varied from 15dB to 35dB, where ten unique packets are sent per SNR trial and the channel parameters (150ns of delay spread, according to an exponential Rayleigh channel model and nulls are limited to a depth of 15 dB) are unique for each trial. Unless otherwise noted the CFO is 15ppm. Using only the received Long Training Sequences of fully-compliant IEEE802.11a packets, both the TX and RX I/Q imbalance parameters are estimated on a packet-by-packet basis (i.e. without the need for a convergence period).

Several packet-switching capable algorithms are considered and compared in this study: Ideal Correction, LLSE using a simple frequency domain equalizer (as described in [Fei08]), LLSE using the improved equalization technique, CLSE estimation using a serial single-dimension numerical search (using the LLSE results as the starting point), CLSE using the Newton-Raphson algorithm (also using the LLSE results as the starting point), and no correction. For the results presented in Figure 1, a TX I/Q imbalance of  $0.8dB$  in amplitude and  $5^\circ$  in phase and the RX I/Q imbalance of  $-0.9dB$  in amplitude and  $5^\circ$  in phase are used. For the results in Figure 2, a CFO of 15ppm was used. It is observed that there is approximately a 5 dB enhancement in SINR by using the improved but numerically intensive, equalization technique. Though the LLSE technique is effective in reversing the direct conversion-induced distortion, further enhancements are gained by fine-tuning the TX and RX I/Q imbalance parameters through the CLSE technique. It is also observed that both the serial single-dimensional parameter search and the Newton-Raphson estimation techniques yield similar results.

Figure 2 shows the results of the algorithm presented in this paper (using the Newton-Raphson technique) with [Xin05] and a genie-aided approach using the correction technique

presented in [Tan07]. A unique channel response is generated from the exponential Rayleigh model (delay spread of 150ns) for each packet and a 15ppm CFO is applied. Additionally, the TX imbalance parameters are  $.5dB/5^\circ$ , and the RX imbalance is  $-.9dB/5^\circ$ . It is observed that the proposed algorithm restores the received waveform to about .5 dB within ideal over most of the SNR range. [Tan07], which operates under a synchronous channel, and [Xin05] which is intended for scenarios where the TX I/Q imbalance can be ignored, do not converge under these circumstances.

In Figure 3 we provide a comparison between the proposed algorithm (using the Newton-Raphson technique) and simulated performance of [Tan07] under multiuser packet-switching conditions. For this study the RX I/Q imbalance parameters remain constant at  $-.9dB/5^\circ$  while the TX imbalance is uniformly distributed between the interval  $[-1, 1]dB$  and  $[-5, 5]$  degrees. The results in Figure 3 show that while [Tan07] also considers asynchronous TX and RX I/Q imbalance in the presence of multipath, the dynamic nature of the multi-user channel does not allow the convergence loop to estimate either multipath channel parameters or TX I/Q imbalance parameters (both change on a packet-by-packet basis, and it is assumed that each 802.11a packet provides two updates to the estimated per packet). The parameters of [Tan07] are simulated such that its estimator variables are preset to ideal (this demonstrates why the packet-switched multiuser scenario imposes unique algorithmic requirements), then each subsequent packet has a unique set of I/Q imbalance and multipath parameters.

## 5. Conclusions

The multiuser packet-switched scenario creates a situation where, in the case of direct conversion transceivers, critical parameters change on a packet-by-packet basis. This work presents a system model that incorporates the relevant parameters, then presents an improved performance solution to this problem. Simulation results show that this technique successfully removes both TX and RX I/Q imbalance in the presence of (or lack of) CFO and multipath, with results that are close to ideal.

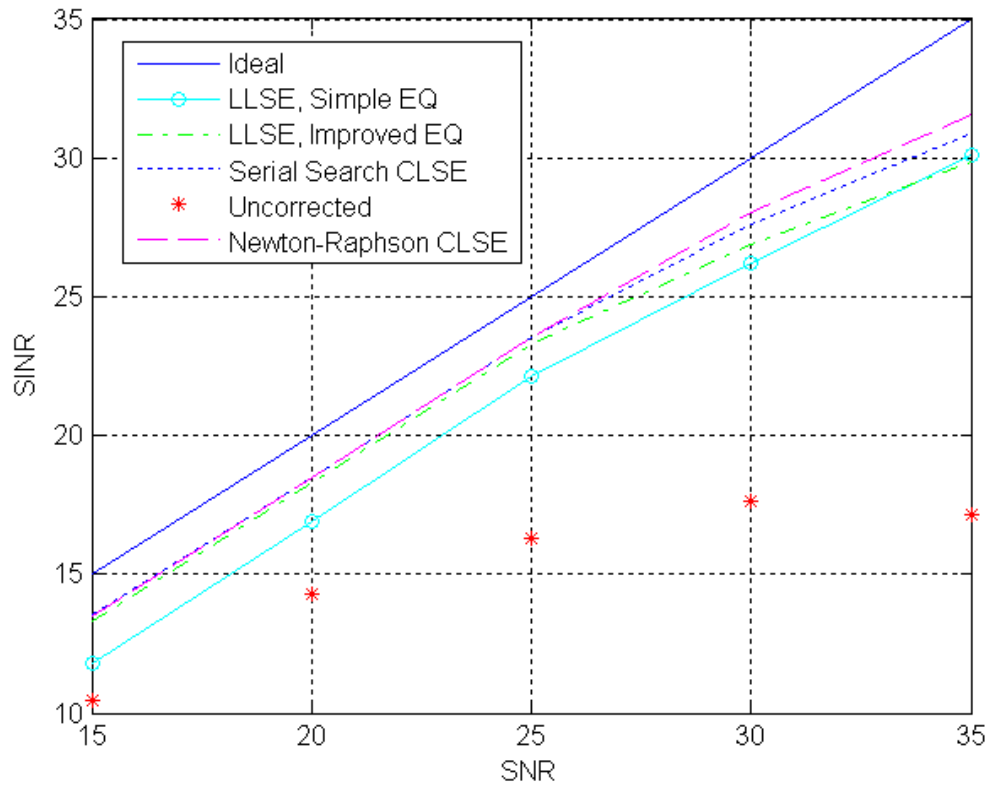


FIGURE 1. Output SINR vs. SNR for various correction schemes using 802.11a OFDM Modulation in the presence of 150nS of multipath delay spread,  $.8dB/5^\circ$  TX I/Q imbalance, and  $-.9dB/5^\circ$  RX I/Q imbalance, and a 15 ppm frequency rotation.

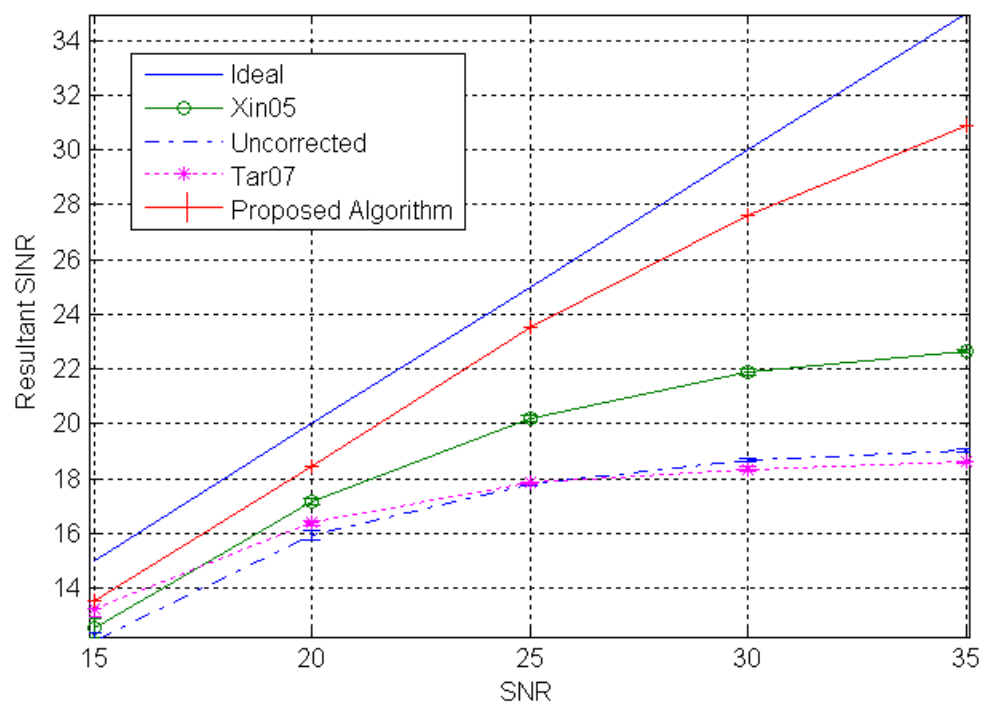


FIGURE 2. Comparison of Output SINR vs. SNR for the proposed correction scheme versus various other works, when applied to this particular system model. This simulation includes 150ns of multipath delay spread,  $.5dB/5^\circ$  TX I/Q imbalance, and  $-.9dB/5^\circ$  of RX I/Q imbalance, and a 15 ppm frequency offset.

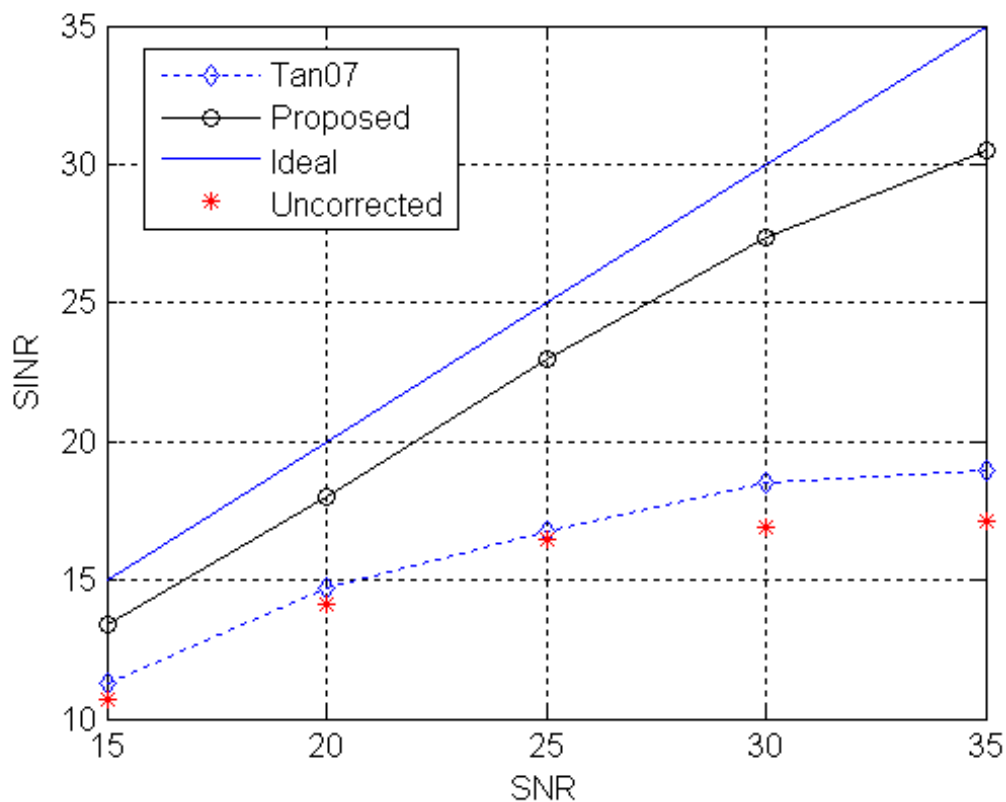


FIGURE 3. This simulation, unlike those represented in the previous figures, considers the multiuser scenario where each received packet emanates from a different TX. The RX I/Q imbalance parameters are  $-0.9\text{dB}/5^\circ$  while each packet has a TX I/Q imbalance that is uniformly distributed between the interval  $[-1, 1]\text{dB}$  and  $[-5, 5]$ degrees. It is shown, according to the resultant output SINR versus input SNR, that the multiuser packet-switched scenario requires critical algorithmic consideration for proper operation.

## CHAPTER 4

# A Solution for Frequency Dependent I/Q Imbalance

### 1. Introduction

This chapter further enhances the system model to include the parameters that account for frequency dependent I/Q amplitude imbalance. Though this effect is less relevant than frequency independent imbalance, primarily due to the fact that circuit design techniques exist to mitigate this problem, there exists the possibility for a signal processing solution that completely removes this effect. As analog circuitry on integrated processes consumes expensive die area, while digital circuitry scales according to 'Moore's Law', it is very cost effective to relax the analog filter design tolerances (relative tolerances of analog circuit elements is related to that components die area) in favor of digital correction. However, such digital correction must remain transparent and implementation independent (i.e., not require manufacturing test and calibration or special hardware design consideration ) in order to obtain maximum benefit. This means that the proposed solution operates within the digital baseband processor of the RX and the only available stimulus waveforms are those received under ordinary operating conditions.

Since this work is intended to operate within the WLAN scenario, where multiple users share the same channel, IEEE802.11a OFDM modulation [IEE99] (also used by 802.11g) is considered the relevant waveform. Each incoming packet suffers a unique Carrier Frequency Offset (CFO), multipath channel parameters, and TX I/Q imbalance, while received in the presence of RX I/Q imbalance (in addition to that caused by this frequency-dependent phenomenon). Therefore, this non-obtrusive algorithm must consider these distortions in its estimation of frequency dependent amplitude imbalance.

The primary cause of frequency dependent imbalance is the fact that the baseband RX filters, whose function are to remove potentially large off-channel signals, are implemented as separate I-channel and Q-channel high order analog filters. Common filter types are Chebyshev Type II and Butterworth (these choices minimize group delay distortion with respect to the amount of rejection provided) whose orders typically range from four to eight. Such filters, especially when made programmable to accommodate a variety of modulation formats and bandwidths, tend to skew from one another.

Analog filters achieve the desired s-plane pole and zero response by a variety of techniques; common integrated circuit methods include Sallen-Key, Tow-Thomas, and Gm-C, all of which rely upon a precise relationships between elements such as current sources, voltage sources, resistors, and capacitors. Finite implementation accuracy results in errors among the locations of the poles and zeros. This results in a shifted magnitude/phase response and a non-ideal magnitude/phase response (with respect to the particular filter prototype).

Works [Tan07, Tar07] considers frequency dependent I/Q imbalance, but in the context of a system model where all packets are received from the same TX (to receive enough training sequences and to ensure a very slowly changing channel for loop convergence), and considers each subcarrier individually. [Tan07] further includes the effects of a static CFO. [Bar07, Lin08] considers frequency dependent I/Q imbalance (also on a carrier-by-carrier basis), but do not consider or correct the effects of the TX I/Q imbalance, as WLAN networks usually contain direct conversion TX's as well as RX's. While such system models exists in many scenarios, they are not applicable to the multiuser WLAN environment. Furthermore, as 4th to 8th order analog filters exhibit a far slower change in magnitude and phase than that of a signal produced by a 64 point IFFT (i.e., OFDM), there exists a large amount of correlation between subcarriers when considering filter mismatch.

Distortion, in terms of phase and magnitude, that is common to both the I-channel and Q-channel filters, is the same linear distortion function as that induced by a quasi static dispersive multipath channel. Residual of the common mode error is removed by even the

basic channel equalizer. The differential distortion between the I-channel and the Q-channel, which is much smaller in magnitude than that of the common mode, is responsible for frequency dependent imbalance. In previous works [Fei08, Fei08a], frequency independent imbalance is considered, which indicates that only the mean of frequency dependent errors are removed. As a comparison, frequency independent imbalance commonly exists at a level of approximately 1 dB, while the more subtle frequency dependent residual (zero mean) effects vary across the channel bandwidth over a range of approximately +/- .25 dB (peak to peak) for WLAN type integrated circuit implementations.

## 2. System Model

Considering that the complex components of the baseband waveform present at the RX are processed by parallel, but somewhat unequal analog lowpass filters, the resultant complex envelope at the receiver's baseband (rotated such that the phase of the desired component is equal to that of the I-branch of the TX) may be written as

$$(52) \quad \begin{aligned} z_R(t) = & h \star k_1 \star z(t) + h \star k_2 \star z^*(t) + \\ & [r^*(t)]^2 h^* \star k_3 \star z^*(t) + [r^*(t)]^2 h^* \star k_4 \star z(t), \end{aligned}$$

where

$$(53) \quad \begin{aligned} k_1(t) &= \frac{1}{4}(\delta(t) + (\delta(t) + \gamma(t))e^{-j\theta_R})(1 + (1 + a_T)e^{j\theta_T}), \\ k_2(t) &= \frac{1}{4}(\delta(t) + (\delta(t) + \gamma(t))e^{-j\theta_R})(1 - (1 + a_T)e^{j\theta_T}), \\ k_3(t) &= \frac{1}{4}(\delta(t) - (\delta(t) + \gamma(t))e^{j\theta_R})(1 + (1 + a_T)e^{-j\theta_T}), \text{ and} \\ k_4(t) &= \frac{1}{4}(\delta(t) - (\delta(t) + \gamma(t))e^{j\theta_R})(1 - (1 + a_T)e^{-j\theta_T}), \end{aligned}$$

Function  $\gamma(t)$  is an acausal, real, impulse response that represents the variation in the amplitude imbalance due to differences in the I- and Q-channel filters. As this amplitude

imbalance variation is gradual across the pass band, a time-domain function best represents such a large coherence bandwidth. The time domain ripple  $\gamma(t)$  is

$$(54) \quad \gamma(t) = a_R g(t) + \sum_{\substack{k = -P \\ k \neq 0}}^P \gamma_k g(t - k).$$

Useful examples of  $g(t)$  include  $B \text{sinc}(tB)$ , where  $B$  denotes the transmission bandwidth, and  $g(t) = \sqrt{B/2\pi} \exp(-B/2t^2)$ . Figure 1 demonstrates the various orthogonal frequency domain results for each values of  $\gamma_k(k_i)$ , where

$$\gamma_k(k_i) = \begin{bmatrix} 0 & 0 & 0 & \underline{x} & 1 & 0 & 0 \end{bmatrix}, \\ \begin{bmatrix} 0 & 0 & 0 & \underline{x} & 0 & 1 & 0 \end{bmatrix} \text{ and} \\ \begin{bmatrix} 0 & 0 & 0 & \underline{x} & 0 & 0 & 1 \end{bmatrix}$$

and the underlined tap indicated the zero-delay value (which is not considered according to equation 54). This shows this functions suitability as a representation of frequency domain coherence and ripple. Further, the fact that each parameter is orthogonal eases estimation.

Using a tap delay line model, the convolution of  $h$  with any vector  $x$ , is represented as

$$(55) \quad h \star x(nT) = x(nT)h_0 + x(nT - T)h_1 + \dots x(nT - LT)h_L \\ = \underline{h}^T \underline{x}(nT)$$

where  $h^T = h_0, h_1 \dots h_L$ . Now, the convolutions terms of equation (52) are represented as

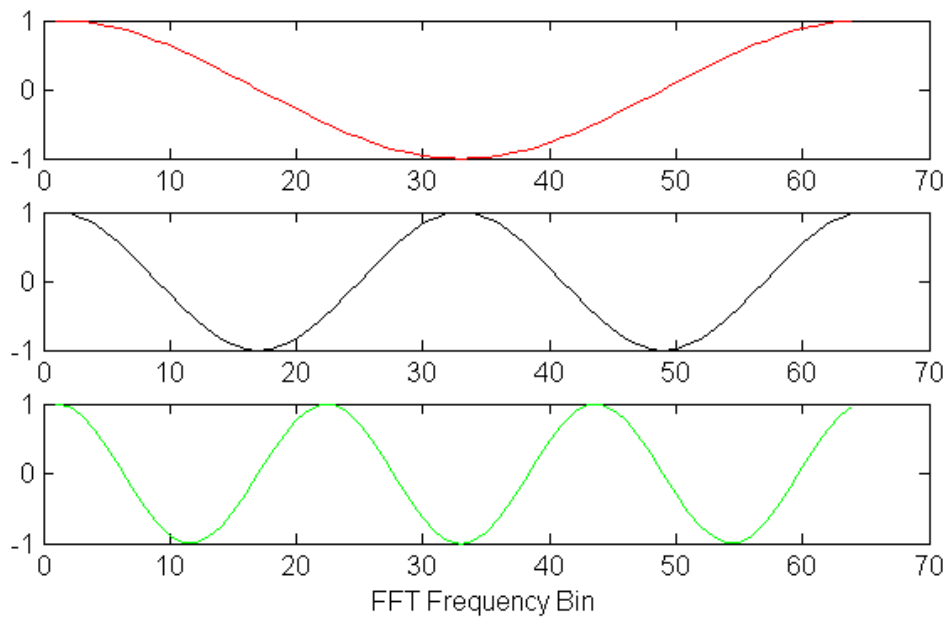


FIGURE 1. Various Orthogonal Frequency Domain Results for the  $\gamma$  Delay Tap Parameters where Only One Tap is Populated with a One. This Demonstrates that the Time Domain Delay-Tap Model is an Effective Means to Exploit Frequency Coherence and is Well-Suited for Ripple Functions.

$$\begin{aligned}
(56) \quad h \star k_1 \star z(t) &= \frac{1}{4} \left[ (1 + e^{-j\theta_R}) \underline{h}^T \underline{z}_t + b^T z_t e^{-j\theta_R} (1 + (1 + a_T e^{j\theta_T})) \right] \\
h \star k_2 \star z^*(t) &= \frac{1}{4} \left[ (1 + e^{-j\theta_R}) \underline{h}^T \underline{z}_t^* + b^T z_t^* e^{-j\theta_R} (1 - (1 + a_T e^{j\theta_T})) \right] \\
h^* \star k_3 \star z^*(t) &= \frac{1}{4} \left[ (1 - e^{j\theta_R}) \underline{h}^H \underline{z}_t^* - b^H z_t^* e^{j\theta_R} (1 + (1 + a_T e^{-j\theta_T})) \right] \\
h^* \star k_4 \star z(t) &= \frac{1}{4} \left[ (1 - e^{j\theta_R}) \underline{h}^H \underline{z}_t - b^H z_t e^{j\theta_R} (1 - (1 + a_T e^{-j\theta_T})) \right]
\end{aligned}$$

where, by considering equation (55),

$$(57) \quad \underline{b}^T \underline{z}_t = h \star \gamma(t) \star z(t)$$

such that  $b$ , the convolved product  $h \star \gamma(t)$ , is  $[b(0), b(1) \dots b(T)]^T$  and  $\underline{z}_t$  is  $[z(t), z(t_1) \dots z(t - T)]^T$ .

### 3. Estimation Approach

The observation,

$$(58) \quad y(t) = \widetilde{Z_R(t)} + w(t), \quad t = 0, 1 \dots N$$

is sampled in discrete time where  $w(t)$  represents Gaussian white noise samples, and  $\widetilde{Z_R(t)}$  is reconstructed as a function of both  $t$  and the unknown parameter vector  $\underline{v}$ , as to minimize the cost function

$$(59) \quad J(\underline{v}) = \left\| y(t) - \widetilde{Z_R(t, \underline{v})} \right\|^2.$$

This estimation operation occurs during the LTS interval, where the undistorted  $z(t)$  is a known sequence. The minimization is performed using the gradient-descent technique by iterating  $\underline{v}$  (the initial values is determined from the LLSE presented in Chapter 2), and  $z$  is the iteration number while  $\mu$  is the step-size:

$$(60) \quad \underline{v}_{z+1} = \underline{v}_z - \mu \nabla J(\underline{v}_z).$$

In this work,  $\mu$  is set to .2 and 100 iterations are performed. Figure 2 shows the progression of the convergence versus iteration number for various SNRs. It is observed that the majority of MSE converges within about 10 iterations, while convergence continues to progress extremely slowly beyond this point.

The  $\nabla J(\underline{v})$  is comprised of  $i$  individual derivatives as

$$(61) \quad \frac{dJ}{dv_i} = -2Re \left[ \left( \frac{d}{dv_i} \widetilde{Z_R(t, \underline{v})} \right) \left( y^*(t) - \widetilde{Z_R^*(t, \underline{v})} \right) \right]_t$$

and

$$(62) \quad \frac{d}{dv_i} \widetilde{Z_R(t, \underline{v})} = \frac{d}{dv_i} h \star k_1 \star z(t) + \frac{d}{dv_i} h \star k_2 \star z^*(t) + [r^*(t)]^2 \left( \frac{d}{dv_i} h^* \star k_3 \star z^*(t) + \frac{d}{dv_i} h^* \star k_4 \star z(t) \right)$$

Considering that for any real or imaginary component of a channel tap or real RX parameter  $v$ ,

$$(63) \quad \begin{aligned} \frac{d}{dv} h \star k_1 \star z(t) &= \frac{1}{4} \left[ \frac{d}{dv} \left( (1 + e^{-j\theta_R}) h^T \underline{z}_t + \frac{d}{dv} (e^{-j\theta_R}) b^T \underline{z}_t \right) \right] [1 + (1 + a_T e^{j\theta_T})] \\ \frac{d}{dv} h \star k_2 \star z^*(t) &= \frac{1}{4} \left[ \frac{d}{dv} \left( (1 + e^{-j\theta_R}) h^T \underline{z}_t^* + \frac{d}{dv} (e^{-j\theta_R}) b^T \underline{z}_t^* \right) \right] [1 - (1 + a_T e^{j\theta_T})] \\ \frac{d}{dv} h^* \star k_3 \star z^*(t) &= \frac{1}{4} \left[ \frac{d}{dv} \left( (1 - e^{+j\theta_R}) h^H \underline{z}_t^* + \frac{d}{dv} (e^{-j\theta_R}) b^H \underline{z}_t^* \right) \right] [1 + (1 + a_T e^{-j\theta_T})] \\ \frac{d}{dv} h^* \star k_4 \star z(t) &= \frac{1}{4} \left[ \frac{d}{dv} \left( (1 - e^{+j\theta_R}) h^H \underline{z}_t + \frac{d}{dv} (e^{-j\theta_R}) b^T \underline{z}_t \right) \right] [1 - (1 + a_T e^{-j\theta_T})] \\ \frac{d}{dRe[h_i]} b(t) &= a_R g(t-l) + \sum_{k=1}^P \gamma_k g(t-k) \\ \frac{d}{dIm[h_i]} b(t) &= j a_R g(t-l) + \sum_{k=1}^P \gamma_k g(t-k) \\ \frac{d}{d\gamma_k} b(t) &= \underline{h}^T g_{t-k}, \quad k = 1, \dots, P \end{aligned}$$

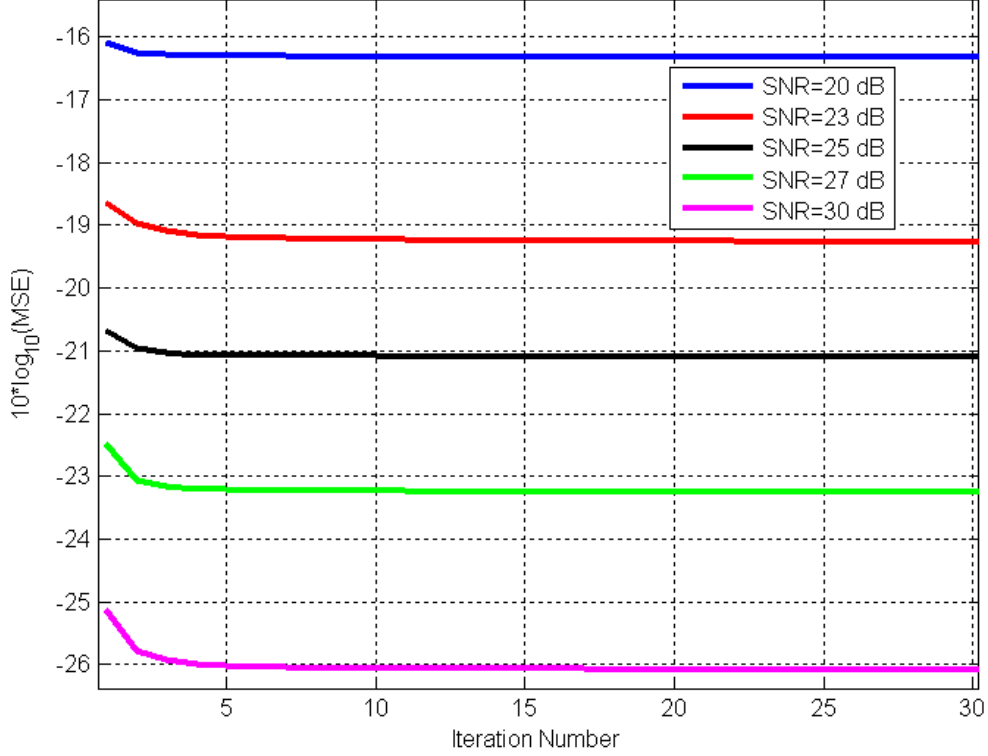


FIGURE 2. The Convergence Behavior of the Gradient Descent Algorithm at Various SNRs.

and  $g'_t = [g'(t), g'(t-l) \dots g'(t-L)]^T$ . If  $v$  is a TX parameter, then

$$\begin{aligned}
 \frac{d}{dv} h \star k_1 \star z(t) &= \frac{1}{4} \left[ (1 + e^{-j\theta_R}) h^T \underline{z}_t + (e^{-j\theta_R}) b^T \underline{z}_t \right] \cdot \frac{d}{dv} \left[ 1 + (1 + a_T e^{j\theta_T}) \right] \\
 \frac{d}{dv} h \star k_2 \star z^*(t) &= \frac{1}{4} \left[ (1 + e^{-j\theta_R}) h^T \underline{z}_t^* + (e^{-j\theta_R}) b^T \underline{z}_t^* \right] \cdot \frac{d}{dv} \left[ 1 - (1 + a_T e^{j\theta_T}) \right] \\
 \frac{d}{dv} h^* \star k_3 \star z^*(t) &= \frac{1}{4} \left[ (1 - e^{+j\theta_R}) h^H \underline{z}_t^* + (e^{-j\theta_R}) b^T \underline{z}_t^* \right] \cdot \frac{d}{dv} \left[ 1 + (1 + a_T e^{-j\theta_T}) \right] \\
 \frac{d}{dv} h^* \star k_4 \star z(t) &= \frac{1}{4} \left[ (1 - e^{+j\theta_R}) h^H \underline{z}_t + (e^{-j\theta_R}) b^T \underline{z}_t \right] \cdot \frac{d}{dv} \left[ 1 - (1 + a_T e^{-j\theta_T}) \right]
 \end{aligned} \tag{64}$$

#### 4. Compensation Algorithm

The received signal,  $z_R(t)$ , is corrected in reverse order as the distortions occurred, as described in the following steps:

1) Frequency Independent RX I/Q imbalance is corrected; It is particularly important that the Quadrature Phase Error is removed in this step:

$$(65) \quad \widehat{z_{R_1}(t_i)} = \left( \text{Re}(\tilde{z}(t_i)) + \text{Im}(\tilde{z}(t_i))\tan(\tilde{\theta}_R) + j\text{Im}\{\tilde{z}(t_i)\} \left( \cos(\tilde{\theta}_R)\tilde{a}_R \right)^{-1} \right)$$

2) Frequency Dependent Amplitude Imbalance is now removed by an Infinite Impulse Response Function (IIR), whose taps (or closest stable taps) are  $\widehat{\gamma}(t_i)$ , and the phase/frequency offset is derotated according the estimation technique presented in [Fei08]:

$$(66) \quad \widehat{z_{R_1}(t_i)} = \widehat{r}^*(t_i) \left( \text{Re} \left\{ \widehat{z_{R_1}(t_i)} \right\} + j\text{Im} \left\{ \text{IIR} \left[ \widehat{z_{R_1}(t_i)} \right] \right\} \right)$$

3) The channel distortion is mitigated linearly in the frequency domain ( symbol ./ denotes component-wise division):

$$(67) \quad \text{FFT} \left( \widehat{z_T(t)r^*(t)} \right) = \text{FFT} \left( \left\{ \widehat{z_C(t)r^*(t)} \right\} \right) ./ \text{FFT} \left( [\tilde{h}_0 \dots \tilde{h}_L \mathbf{0}_{N-L}] \right).$$

4) The derotated TX I/Q imbalance is corrected in the frequency domain:

$$(68) \quad \text{FFT} \left( \widehat{z(t)} \right) = \sum_{r=1}^{N-1} \left( (1 + (1 + \tilde{a}_T)e^{j\tilde{\theta}_T}) \right)^{-1} \left[ \widehat{Z_{T0}}(b) - \left( (1 - (1 + \tilde{a}_T)e^{j\tilde{\theta}_T}) \widehat{Z}^*(L - b) \right) \right],$$

where  $\widehat{Z_{T0}}(b)$  represents the FFT of  $\widehat{z_T(t)r^*(t)}$  at spectral bin  $b$ . Finally, in the next section, this procedure is applied to simulated signals and plotted in comparison with other algorithms.

## 5. Simulation Results

A sequence of fully compliant (bit-level accurate) 802.11a packets are generated and applied to the direct conversion transmitter, receiver, and channel model. As is probable in all WLAN scenarios where multiple users occupy the same wireless spectra (intentionally or unintentionally), each received Physical Layer packet is modeled with unique TX I/Q

Imbalance, CFO and Rayleigh Channel parameters. TX imbalance is uniformly varied over a range of  $[-.3 \ .3]$ dB,  $[-5 \ 5]$  degrees, the CFO is uniform over the interval  $[-40 \ 40]$  ppm (the carrier frequency is considered to be 5.8 GHz), and the channel is implemented using a Rayleigh Delay-Tap model whose RMS Delay Spread is 150 ns and nulls are limited to 15 dB.

As the estimation and compensation algorithms always remain connected to the same direct conversion receiver, RX parameters remain static:  $.9$  dB, and  $-5$  degrees with various degrees of amplitude imbalance across the passband. In-line (pre-estimation) correction is employed according to historical results and thus conventional CFO estimation is utilized since I/Q imbalance-dependent estimation errors diminish after reception of only a 1-2 suitable packets (which could have been received at any point since the radio was manufactured). Full parameter estimation is employed for those packets whose CFO is greater than 25 KHz (4 ppm), while historical receiver I/Q imbalance results are used when the CFO is small.

Each simulation point represents a single SNR, where Signal is defined as the power of the desired components of the transmitted signal and Noise is the circular symmetric AWGN applied to the antenna of the RX. The  $\gamma(t_i)$  portion of the estimation algorithm is seeded with the averaged result of 5 suitable received packets where the SNR was 15 dB and the results of each simulation run are then averaged into the running estimate to seed the next estimation. Figure 3 shows a comparison of estimation results at various SNRs as well as the averaged result of five packets at a 15 dB SNR. The correction algorithm directly utilizes the output of the estimation algorithm, without direct consideration of the historical results or averaging.

Figure 4 shows the simulation results of the various algorithms presented in Chapters 2 and 3, in comparison with this technique. Here, a  $\pm .5$  dB peak sinusoidal frequency-dependent I/Q amplitude imbalance is included in the RX model to demonstrate a large baseband filter error. It is observed that the LLSE technique is somewhat effective in removing this distortion, but suffers a large constant offset from the ideal result. Similarly, the

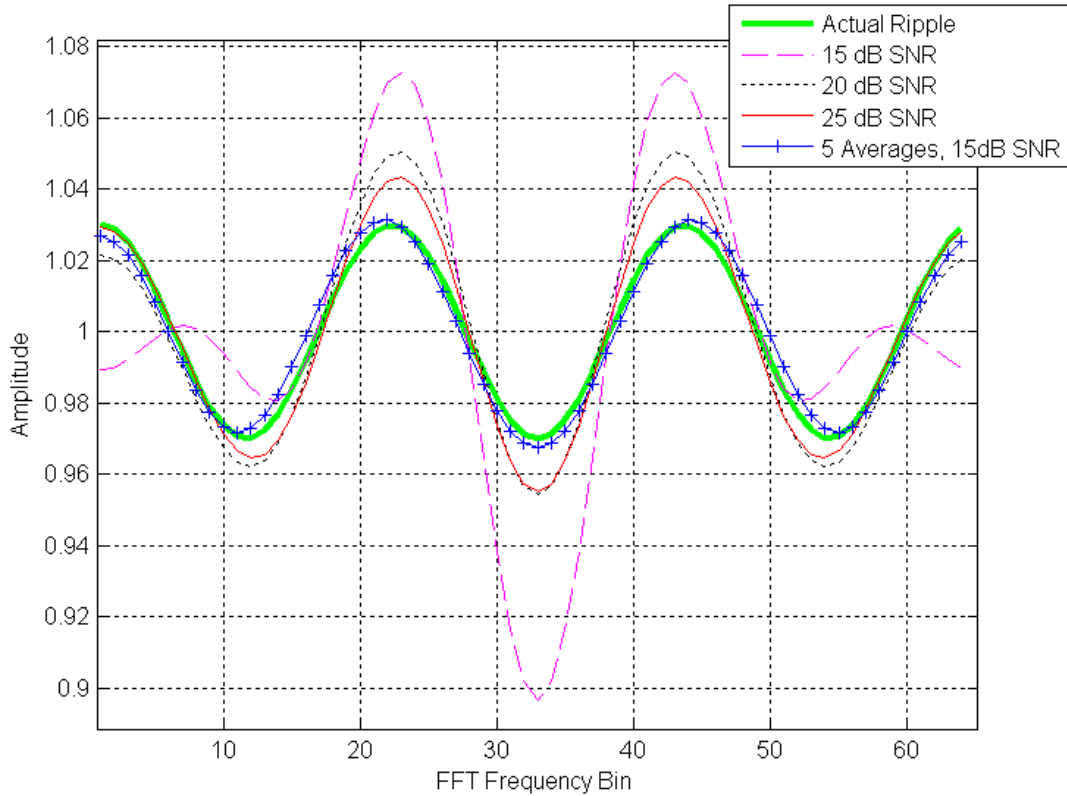


FIGURE 3. The Results of of Frequency Dependent Imbalance Estimation versus the Actual Imbalance are shown at Various SNRs. It is Also Shown that the Averaged Result of Five Unique Estimates at an SNR of 15 dB Provides an Excellent Estimate.

frequency independent CLSE as well as the LLSE with improved equalizer also suffer a large offset and show an output SINR ceiling at the high input SNRs; This behavior is attributed to equalization error due to the fact that these algorithms do not consider frequency dependent imbalance and the equalization results suffers. It is further observed that the CLSE algorithm offers very little advantage of LLSE in the presence of this strong frequency dependent I/Q amplitude imbalance. Finally, it is shown that the proposed algorithm effectively tracks the input SNR, hence is effective at removing the distortion.

Figure 5 shows the simulation results for a mild frequency dependent I/Q amplitude imbalance of  $\pm 0.1$  dB. Here, it is observed that there exists a clear advantage for CLSE than LLSE, but both are subject to an output SINR ceiling. It is also shown that the proposed

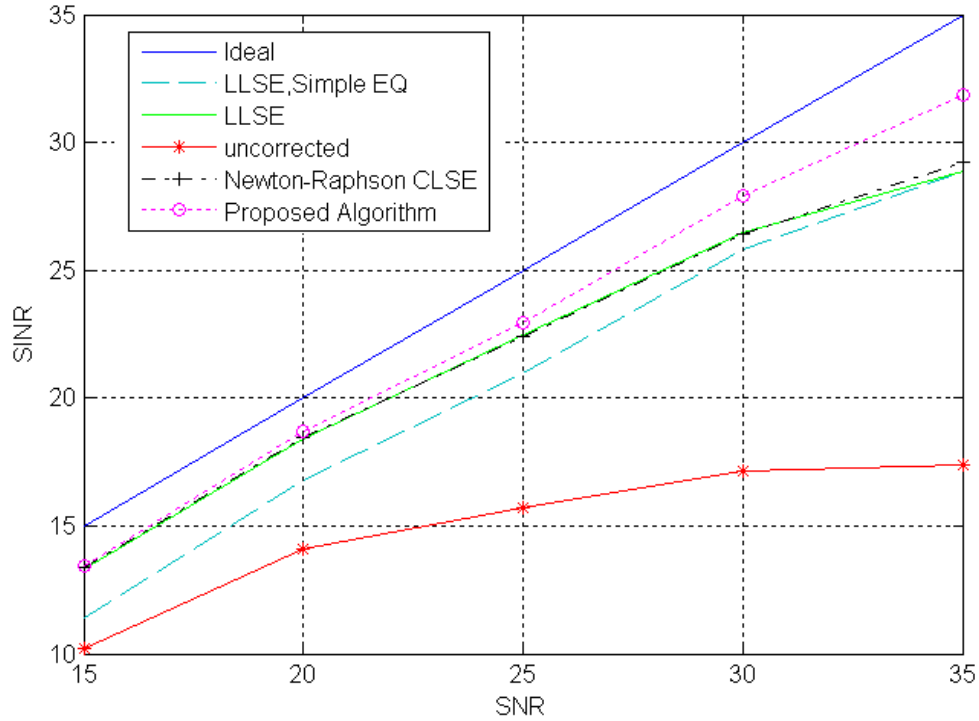


FIGURE 4. Simulation Results for Various I/Q Imbalance Correction Algorithms in the Packet Switched Scenario where the RX Contains Severe ( $\pm 0.5$  dB) of Frequency Dependent Amplitude Imbalance Across the Channel Bandwidth.

algorithm is also effective, even in the presence of mild frequency dependent amplitude imbalance.

Finally, Figure 6 shows a comparison with another algorithm, [Tan07]. This particular algorithm uses an LMS-based approach that includes all of the parameters as this the proposed system model, but does not account for the packet switching scenario. It is shown that this algorithm cannot track the various parameters that change on a packet-by-packet basis, while the proposed algorithm is capable.

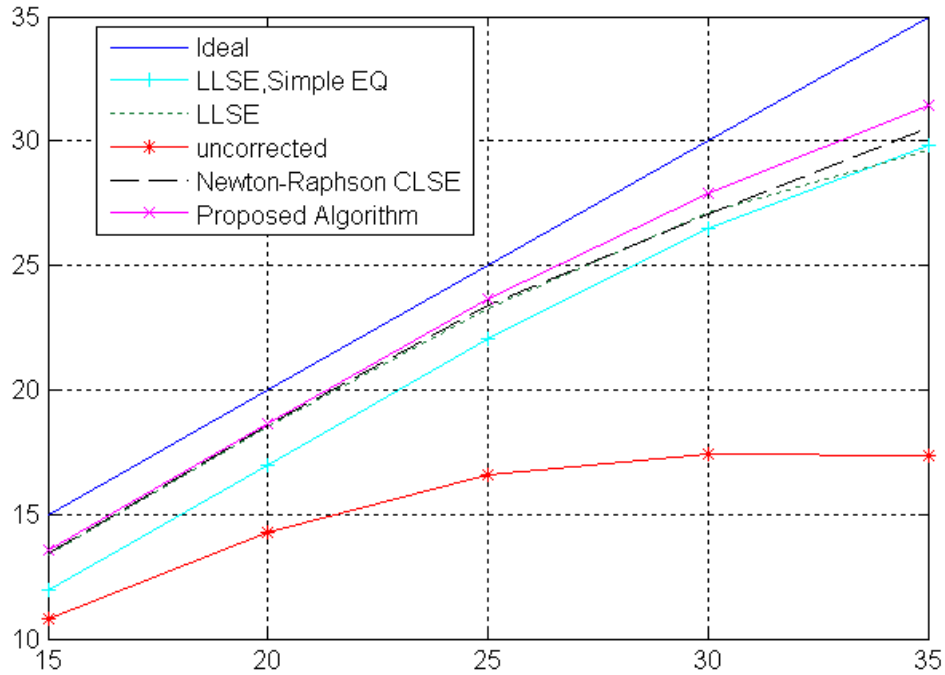


FIGURE 5. Simulation Results for Various I/Q Imbalance Correction Algorithms in the Packet Switched Scenario where the RX Contains Mild ( $\pm 0.1$  dB) of Frequency Dependent Amplitude Imbalance Across the Channel Bandwidth.

## 6. Conclusions

A high performance fully compliant 802.11a I/Q imbalance correction algorithm that includes TX error, RX error, CFO, multipath, and frequency-dependent RX amplitude imbalance has been presented. It has been shown that this algorithm is capable of tracking dynamic TX parameters, CFO, and channel parameters that change on a packet-by-packet basis, while maintaining an utilizing historical RX imbalance parameters. This algorithm, unlike others, is believed to be the only deployable I/Q imbalance correction scheme for the WLAN scenario where, both the TXs and the RXs are direct conversion.

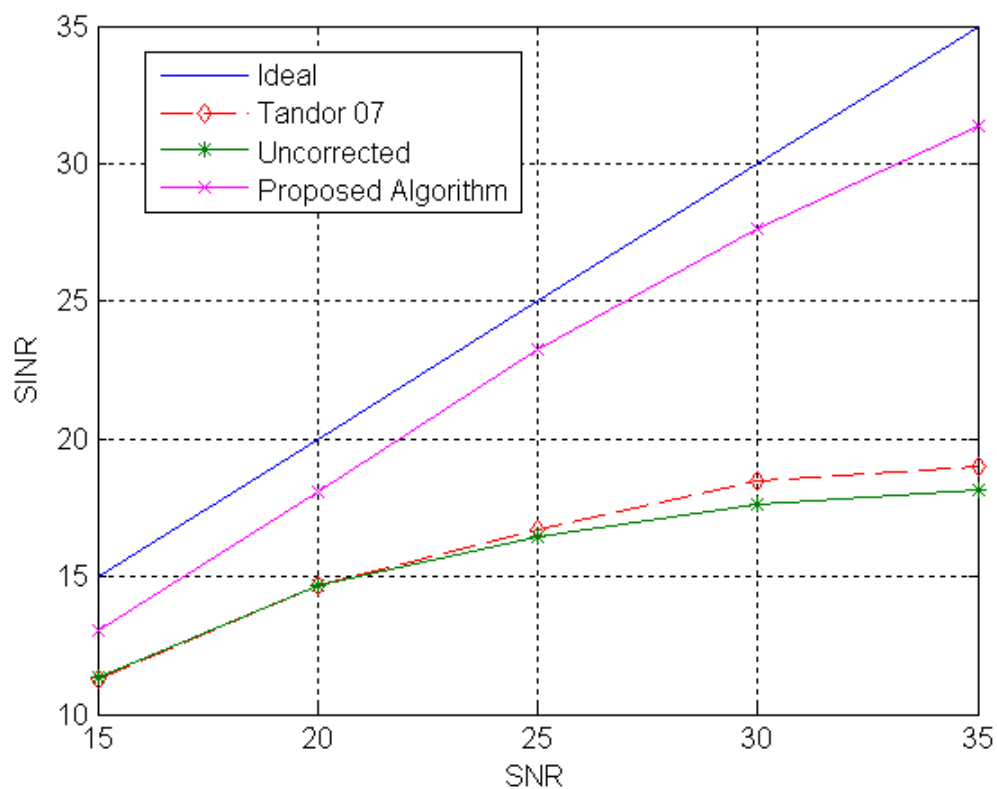


FIGURE 6. A Comparison of the Proposed Algorithm and Tandor07 in the Packet Switched Scenario where the RX Contains Severe ( $\pm 0.5$  dB) of Frequency Dependent Amplitude Imbalance Across the Channel Bandwidth.

## Bibliography

- [Bar07] I. Barhumi, M. Moonen, "IQ Imbalance Compensation for OFDM in the Presence of IBI and Carrier Frequency Offset," *IEEE Trans, on Signal Proc.*, Vol. 55, No.1, Jan. 2007, pp 256-266.
- [Chi06] Shih-Chieh Yen; Ying-Yao Lin, et. al. "A Low-Power Full-Band 802.11abg CMOS Transceiver with On-Chip PA", Radio Frequency Integrated Circuits (RFIC) Symposium, 2006 IEEE
- [Cou07] L.W. Couch II, *Digital and Analog Communication Systems*, 7<sup>th</sup> edition, Pearson/Prentice Hall, p.241.
- [Fei08] Chapter Two of this work, In Second Revision at *IEEE Trans, on Signal Proc*
- [Fei08a] Chapter Three of this work, Not Yet Submitted
- [Fou02] S. Fouladifard , H Shafiee, "Frequency offset estimation in OFDM systems in presence of IQ imbalance", IEEE ICC'02
- [Hai07] Carrier Frequency Offset and I/Q Imbalances Compensation in OFDM Systems Hai Lin; Adachi, T.; Yamashita, K.; Global Telecommunications Conference, 2007. GLOBECOM '07. IEEE 26-30 Nov. 2007 Page(s):2883 - 2888
- [Hai08] Joint Compensation of Frequency-Selective I/Q Imbalance and CFO in OFDM-Based WLAN Hai Lin; Nakao, T.; Yamashita, K.; Consumer Communications and Networking Conference, 2008. CCNC 2008. 5th IEEE 10-12 Jan. 2008 Page(s):388 - 392
- [Hei02] J. Heiskala, J. Terry, "OFDM Wireless LANs: A Theoretical and Practical Guide," 2<sup>nd</sup> edition, Sams Publishing, p.77.
- [IEE99] Wireless LAN Medium Access Control (MAC) and Physical Layer (PHY) Specification: High Speed Physical Layer in the 5 GHz Band, IEEE 802.11 Task Group a, Part 11, 1999.
- [Lin08] H. Lin, T. Nakao, J. Yamashita, "Joint Compensation of Frequency-Selective I/Q Imbalance and CFO in OFDM-based WLAN", IEEE Consumer Comms. Networking Conf., Jan., 2008
- [Par07] Joint Estimation of Carrier Frequency Offset and I/Q Imbalance for Direct Conversion OFDM System with Constrained Preambles Park, Jonghun; Lee, Yusung; Park, Hyuncheol; Signals, Systems

- and Computers, 2007. ACSSC 2007. Conference Record of the Forty-First Asilomar Conference on 4-7 Nov. 2007 Page(s):1786 - 1790
- [Ryk08] On the Connection of I/Q Imbalance and Channel Equalization in Direct-Conversion Transceivers Rykaczewski, P.; Valkama, M.; Renfors, M.; Vehicular Technology, *IEEE Transactions on* Volume 57, Issue 3, May 2008 Page(s):1630 - 1636
- [Sch06] T. Schenk, P. Smulders, E. Fledderus, "Estimation and Compensation of TX and RX IQ Imbalance in OFDM-based MIMO Systems," *IEEE Radio and Wireless Symposium*, Jan. 2006, pp. 215 - 218
- [Tar07] A. Tarighat, A. Sayed, "Joint Compensation of TX and RX Impairments in OFDM Systems," *IEEE Trans. Wireless Comms.*, Vol. 6., Jan., 2007, pp. 240-247.
- [Tub03] J. Tubbax, B. Come, S. Donnay, et al., "Joint Compensation of IQ Imbalance and Frequency Offset in OFDM Systems," *IEEE Radio and Wireless Conference*, Aug. 2003, pp. 39-42
- [Tan07] D.Tandur, M.Moonen, "Joint Adaptive Compensation of TX and RX IQ Imbalance Under Carrier Frequency Offset in OFDM-Based Systems", *IEEE Trans, on Signal Proc.*, Vol. 55, No. 11, Nov 2007
- [Tub03] J. Tabbax, B. Come, L. Van der Perre, et. al., "Joint Compensation of IQ Imbalance and Frequency Offset in OFDM Systems," in Proc. Radio Wireless Conf. (RWC), 2003, pp.39-42
- [Val01] M. Valkama, M. Renfors, V. Koivunen, "Advanced Methods for I/Q Imbalance Compensation in Communications RXs," *IEEE Trans, on Signal Proc.*, Vol. 49, No. 10, Oct, 2001, pp. 2335-2344
- [Val05] M. Valkama, M. Renfors, V. Koivunen, "Blind I/Q Imbalance Compensation in OFDM RXs Based on Adaptive I/Q Signal Decorrelation," *IEEE Int Sym on Circuits and Systems*, May 2005, vol. 3, pp. 2611 - 2614
- [Val05a] Blind I/Q Signal Separation-Based Solutions for RX Signal Processing Valkama, M; Renfors, M.; Koivunen, V. *EURASIP Journal on Applied Signal Processing* Volume 2005 (2005), Issue 16, Pages 2708-2718
- [Xin05] G. Xing, M. Shen, and H. Liu, "Frequency Offset and I/Q Imbalance Compensation for Direct-conversion Receivers," *IEEE Trans. on Wireless Communications*, VOL. 4, NO. 2, MARCH, 2005, PP. 673-680.
- [Yan07] D.Tandur, M.Moonen, "Joint Adaptive Compensation of TX and RX IQ Imbalance Under Carrier Frequency Offset in OFDM-Based Systems", *IEEE Trans, on Signal Proc.*, Vol. 55, No. 11, Nov 2007F. Yan, et. al "Carrier frequency offset estimation and I/Q imbalance compensation for OFDM systems". *Eurasip Journal on Advances in Signal Processing* Volume 2007 (2007).

- [Yan04] F. Tan, W. Zhu, and M.O. Ahmad, "Carrier Frequency Offset Estimation for OFDM Systems with I/Q Imbalance," in Proc. IEEE 47th Midw. Symp. Circuits Syst., 2004, pp. 633-636
- [Zha05] P. Zhang, Lawrence Der, et. al., "A Single-Chip Dual Band Direct-Conversion IEEE 802.11a/b/g WLAN Transceiver in 0.18 $\mu$ m CMOS", IEEE Journal of Solid-State Circuits, Vol. 40, No.9, Sept.,2005
- [Zou08] Analysis and Compensation of TX and RX I/Q Imbalances in Space-Time Coded Multiantenna OFDM Systems Zou, Y.; Valkama, M; Renfors, M.; EURASIP Journal on Wireless Communications and Networking Volume 2008 (2008), Article ID 391025, 16 pages